TR - O - 0013

48

Electronic structures of GaAs - AlAs superlattices

Shigetoshi NARA
奈良重俊

1989. 8. 30.

ATR光電波通信研究所

Abstract

This is the report which discusses the electronic band structure of microscopic superlatteces with use of an improved tight binding method developed by the author, especially, in GaAs - AlAs system of both (100) and (111) directionsis. The dispersion relation is calculated and the effect of spin - orbit interaction to the states at the top of valence band is discussed in detail. The author predict the anomaly in the optical polarization associated with the absorption or emission of light in (100) and (111) superlattices depending on the atomic layer number combinations (m, n) in the $(GaAs)_m/(AlAs)_n$

Contents

1 Introduction

The electronic structure of superlattices of Ⅲ-Ⅴ semiconductor compounds has been attracting the interest of many workers [1)~11)] * since it enables us to investigate materials from the microscopic view point and to tailor them for engineering applications.

In the previous paper [11)], hereafter referred as Ⅰ, the band structure of $(GaAs)_n/(AlAs)_n$ $(n=1\sim4)$ superlattices was investigated with the use of an improved tight binding method, where " an improved .... " means that the better fitting of the conduction bands as well as the valence bands of the bulk materials to the results of pseudopotential method [12),13)] was obtained (see Fig.1.1) by introducing new parameters in the overlap integrals between the localized basis orbitals which are regarded, usually, as being ortho-normal in the sense of Löwdin's treatment [14)]. The main point of discussion in Ⅰ was about the differences between the band structures of superlattices for the two choices of band offset values, one is Kroemer's [15)] rule and the other Dingle's rule [2)]. However, a detailed discussion of another important effect of superlattices was left, that is, the band folding effect.

In the present paper, based on the same method, the electronic bands of $(GaAs)_n/(AlAs)_1$ and $(GaAs)_1/(AlAs)_n$ $(n=1\sim10)$ are investigated because an artificially arranged periodic potential of one atomic monolayer makes the band folding effect clearly occur especially when the mole fraction of a monolayer compounds is quantitatively less than the other constituent materials of superlattice.

---

* see the references listed in the author's paper (the ref. 11)

It is the second aim of this paper to consider a possibility of transforming the indirect gap materials into the direct gap materials with making use of such a band folding effect.

Finally, in the present examples of material combination of a superlattice structure, the optical oscillator strength is estimated in order to obtain the qualitative feature of optical properties.

2 An improved method of tight binding band structure calculation

We omit the detailed description of the present improved tight binding method to avoid the lengthy expression. The outline of formulation is given in I. Here, our final eigen value problem to be solved is of the form[11),16)]

$$\left| H_{\kappa\kappa'}(\mathbf{k}) - E\, S_{\kappa\kappa'}(\mathbf{k}) \right| = 0, \tag{2.1}$$

where

$$H_{\kappa\kappa'}(\mathbf{k}) = \sum_{l} e^{i\mathbf{k}\cdot\mathbf{R}_l} \int \phi^{*}_{\kappa}(\mathbf{r})\, H\, \phi_{\kappa'}(\mathbf{r}-\mathbf{R}_l)\, dv,, \tag{2.2}$$

$$S_{\kappa\kappa'}(\mathbf{k}) = \sum_{l} e^{i\mathbf{k}\cdot\mathbf{R}_l} \int \phi^{*}_{\kappa}(\mathbf{r})\, \phi_{\kappa'}(\mathbf{r}-\mathbf{R}_l)\, dv, \tag{2.3}$$

$$\mathbf{R}_l = \lambda_l a\,\mathbf{u} + \mu_l b\,\mathbf{v} + \nu_l c\,\mathbf{w}. \tag{2.4}$$

H is the Hamiltonian and $\mathbf{k}$ is the wave vector in the Brillouin zone. $\{\phi_{\kappa}(\mathbf{r})\}$ is the set of atomic valence orbitals of concerning system, where, in the present case, κ are s-, p_x-, p_y- and p_z- orbitals. $\{\mathbf{R}_l\}$ is the set of vectors indicating the configuration of atoms in the given structures, where $\{\lambda_l, \mu_l, \nu_l\}$ is a set of integer. a, b, c and $\mathbf{u}$, $\mathbf{v}$, $\mathbf{w}$ are the lattice constants and the primitive translation vectors of the concerning structure, respectively. We restrict the set

of transfer and overlap integral parameters to the nearest and next nearest neighbor sites for the sake of keeping the global uniqueness of choosing the parameter values.

3 Spin - Orbit Interactions

To include the spin-orbit interaction, we must add the following new term to the Hamiltonian [17]

$$H_{SO} = \Lambda (\nabla Vc \times \mathrm{p}) \bullet \mathrm{s} \tag{3.1}$$

where Vc is the crystal potential, p is the momentum operator, and s is the spin operator. We regard Vc as a spherical symmetric potential, a valid approximation in the band structure calculation. Then (3.1) is

$$H_{SO} = \lambda \ \mathrm{l} \bullet \mathrm{s} \tag{3.2}$$

where l is the angular momentum operator and λ are constant parameters which correspond to the atomic spin-orbit interaction strengths for Al, Ga, As, respectively. λ are chosen to give best fit with the pseudopotential results.[12), 13)]

4 (100) - superlattices

4.1 General properties

In the calculation for $(GaAs)_m/(AlAs)_n$, it should be noted that the space groups are different depending on n, that is,

$$m+n = even \ : \ D_{2d}^{1}$$

$$= odd \ : \ D_{2d}^{11}$$

The Bravais lattie is the simple tetragonal for the former and the body centered tetragonal for the latter. The primitive translation vector for $(GaAs)_2/AlAs)_1$, is shown in Fig.4.2(a) and the corresponding Brillouin zone in Fig.4.2(b) as well as the simple tetragonal Brillouin zone of $(GaAs)_1/(AlAs)_1$ in Fig.4.1.

4.2 Dispersion without spin - orbit interactions

In the results of calculation, the band structure for $(GaAs)_3/AlAs)_1$ is shown in Fig.4.3 in the extended zone scheme, as well as Fig.4.4 (a),(b) for $(GaAs)_4/(AlAs)_1$, $(GaAs)_1/(AlAs)_4$, Fig.4.5 for $(GaAs)_1/(AlAs)_9$, where note that the scale of vertical axis in Fig.4.5 is enlarged for the brevity of showing. The discussion is given in the next section.

In both cases of $(GaAs)_4/(AlAs)_1$, and $(GaAs)_1/(AlAs)_4$, the constitutively dominant component [GaAs in the $(GaAs)_4/(AlAs)_1$, for instance] determines the global band dispersion, which is easily seen in the extended zone scheme as shown in Fig.4.3~4.5, however, the new large band gaps open at the new zone boundary which are due to the new periodic potential introduced by the constitutively less component substance. [AlAs in the $(GaAs)_4/(AlAs)_1$, for instance]. This new band gaps are relatively large near the primary band gap between valence and conduction bands, but becomes smaller at the deeper part of valence bands and at the higher part of conduction bands. These tendencies become stronger in the larger n-values.

In the conduction band, the two important points should be noted. One is that, in $(GaAs)_1/(AlAs)_n$, the direct and indirect minimum gap appears alternately depending on n, where the direct gap is realized when $n=2, 4, 6, 8, 10$ as shown in Fig.4.6(b) although, all through $n = 1 \sim 10$ of this case, the conduction band edge consists dominantly of the X-point or Δ-line states of the original zinc-blend structure if one looks their eigenvectors in detail. The second point is that the conduction band structure indicates rather complicated

dispersion because the bands folded from the original zinc-blend bands results in the crossing at many points in the new Brillouin zone and split off in the superlattice structure, on account for the mutual coupling.

Now the systematic calculation of band gap alternation is shown in Fig. 4.6(a) and 4.6(b) for $(GaAs)_n/(AlAs)_1$, and $(GaAs)_1/(AlAs)_n$, $(n=1\sim10)$, respectively. In the former case, the minimum band gap is direct except only $(GaAs)_1/(AlAs)_1$, and the gap energy quickly approaches the bulk value of GaAs as n increases, on contrasting, in the latter case, the minimum band gap appear near the X-point energy of bulk AlAs and its minimum gap energy alternates between the direct and the indirect gap depending on n, the result of which is interpreted from its folded band structures in the following way. As shown in Fig.4.7, the X [(M)] -point or the intermediate points along the Γ-X [(M)-(M)] -line are folded to the Γ [(M)] -point depending on either even $(n+1)$ or odd $(n+1)$ number, where M means the standard name of high symmetry points in the tetragonal Brillouin zone but the same point is named as X in the body centered tetragonal structure[18] , thus we use (M) both in the simple and body centered tetragonal structures to avoid the confusion of usage when it is described in the present article. Now the calculated eigenvectors of the Γ- and (M)- points of superlattices indicate, which we do not show their actual component data at present, that the amounts of mixing component of GaAs, for instance, in $(GaAs)_1/(AlAs)_3$ and $(GaAs)_1/(AlAs)_4$ are different depending on even $(n+1)$ and odd $(n+1)$, that is, the GaAs-component for $n=3$ is much less than that for $n=4$. It is reflected to the energy level of Γ- and (M)- points as the indirect gap of $(GaAs)_1/(AlAs)_3$ and the direct gap of $(GaAs)_1/(AlAs)_4$. This trend is common for the other values of n, therefore the alternate appearance of direct and indirect minimum band gap occurs

The situation of obtaining the indirect gaps in $(GaAs)_1/(AlAs)_1$ and $(GaAs)_1/(AlAs)_3$ is consistent with the results of more accurate but harder calculations done by, for instances, Nakayama and Kamimura[5] or Saito and

Oshiyama[9] with use of the self consistent pseudopotential method, as well as by Hamada, Ohnishi and Oshiyama[4] with use of the full-potential linearized augmented-plane-wave method (FLAPW) . The coincidence with their results show that the present improved tight binding method is not useless for the rough speculation of new band structure not only for the $(GaAs)_n/(AlAs)_m$ system but also the other combinations between the different III- V compounds, moreover hopefully, even for the combinations between II- VI compounds which are the extended attempt of the present author, however, it should be noted that the present method can not treat the problem of stabilities of thsese new structure, especially, a serious difficulty will occur due to the essential weak point of parameter theory if it includes the lattice mismatched case, while one manages to calculate the band structure as Osbourn[8] had done with employing the lattice distance dependency of patrameters (transfer and overlap). The further comparison for larger n in the present GaAs-AlAs system with more accurate calculations is desirable but unfortunately the detailed *ab initio* investigations with respect to the systematic tendencies of the band gaps as well as the eigenvectors over the wide ranges of the wave vector and the energy in the new Brillouin zones have not yet been reported for the present types ($n:1$ or $1:n$; $4 \leqq n \leqq 10$) of superlattices.

4.3 Oscillator strength between bottom of conduction band and top of valence bands

Finally, the estimated oscillator strength at the Γ-point is shown in Fig.4.8 if the calculated bands have direct minimum gap. Fig.4.8(a) shows the case of $(GaAs)_n/(AlAs)_1$ ($n=2\sim10$) in which the vertical axis is normalized by the value of bulk GaAs. As n increases, the oscillator strength approaches $2/3=0.666\cdots$ asymptotically, which is due to the reason that the valence band top is two fold degenerate on account for the tetragonal symmetry of the present type of superlattice on contrasting the three fold degeneracy of bulk (zinic-blend) GaAs.

The result for $(GaAs)_1/(AlAs)_n$, ($n=2\sim10$) is shown in Fig.4.8(b) and this case indicates that the optical oscillator strength is quite little due to the reason mentioned in the second paragraph in this section, therefore the expected optical properties are much less effective even if one succeeds to make the direct gap materials by the artificial insertion of periodic one monolayer substance in the indirect gap materials. It seems, unfortunately, not so hopeful for an application of superlattices. However, the several possibilities of making the oscillator strength be stronger are retained, for instance, the employing a combination of substances where the large different band characters exist between them will increase the oscillator strength since the Γ-character of folded band increases if the much modification of original symmetry occurs in the superlattice structures, so that, the lattice mismatched case or a combination of semiconductors and ionic materials (Si-Ge or AlAs-CaF_2, for instances) has the strong possibility of realizing a new optically active and tailorable materials. However, the further calculations and experiments are desirable.

4.4 With inclusion of spin - orbit interactions

The calculated bandstructure is shown in Fig.4.9 for the case of $(GaAs)_1/(AlAs)_1$. Note that every level is two fold degenerate and at the Γ-point the heavy hole and the light hole are split by the crystalline tetragonality of the superlattice. The detailed dispersion near the top of the valence band is shown in Fig.4.10 with, for comparison, the dispersion of bulk GaAs and of the superlattice without the spin-orbit interaction. It is important that at the Γ- point the state of the heavy hole is the eigenfunction of the total angular momentum ($J = 3/2, J_z = \pm 3/2$) but the light hole state is not an eigenfunction of the total angular momentum but a mixture of the states ($J = 3/2, J_z = \pm 1/2$) and ($J = 1/2, J_z = \pm 1/2$) due to the crystalline tetragonality of superlattice. One can understand this from the symmetry considerations using group theory. In the case where the

spin-orbit interaction is not considered, the wave function at the top of the valence band in the bulk zinc-blend structure of III-V semiconductor compounds consists of bonding orbitals which are linear combinations of p-orbitals of cation (Ga or Al) and anion (As). These bonding orbitals have the p-orbital like symmetry and belong to the irreducible representation denoted by Γ_5 in the point group T_d at the Γ-point. Let us represent these wave functions by $\{p_i\}$ (i $= x, y,$ and z). When we take the spin orbit interaction into account, we should reduce the direct product between Γ_5 and the spinor $\{\alpha, \beta\}$ into the irreducible double point group of T_d symmetry. The table of characters is given in Table 4.1. The six states [(orbital : 3) $\times$ (spin : 2) = 6] seperate into two states. One is four fold degenerate and the other is two fold degenerate. The former is the eigenstate of total angular momentum with $J = 3/2$ ($Jz = \pm 3/2$ is the heavy hole and $Jz = \pm 1/2$ is the light hole). The latter is the eigenstate of total angular momentum with $J = 1/2$ and is called *the split off band.*

Under the symmetry D_{2d} at the Γ-point of the superlattices and without spin-orbit interaction, these original bonding p-orbitals split into two states,[11] one is two fold degenerate $\Gamma_5 = \{p_x, p_y\}$ and the other is not degenerate, $\Gamma_4 = \{p_z\}$ in the D_{2d} point group. This result is obtained from the reduction of the character $\chi(\{p_i\})$ into the irreducible representation of D_{2d} which is shown in Table 4.2.

The final result for the top of the valence band in the superlattice (D_{2d} symmetry) with inclusion of spin-orbit interaction will be obtained by the reduction of $\Gamma_5 \times \{\alpha, \beta\}$ and $\Gamma_4 \times \{\alpha, \beta\}$. The former gives $\Gamma_6 + \Gamma_7$ and the latter gives Γ_7. Now, the wave function of Γ_6 is the eigenfunction of total angular momentum ($J = 3/2, J_z = \pm 3/2$). However, Γ_7 from the former and Γ_7 from the latter are neither the eigenfuction of ($J = 3/2, J_z = \pm 1/2$) nor ($J = 1/2, J_z = \pm 1/2$), as shown below,

$$\Gamma_5 \times \{\alpha, \beta\} = \Gamma_6 + \Gamma_7 \qquad (4.1)$$

$$\Gamma_6 : \{ (p_x + i p_y)\alpha, (p_x - i p_y)\beta \} \tag{4.2}$$

$$\Gamma_7 : \{ (p_x - i p_y)\alpha, (p_x + i p_y)\beta \} \tag{4.3}$$

$$\Gamma_4 \times \{\alpha, \beta\} = \Gamma_7. \tag{4.4}$$

$$\Gamma_7 : \{ p_z\alpha, p_z\beta \} \tag{4.5}$$

$$(J = 3/2, J_z = \pm 3/2) : \{ (p_x + i p_y)\alpha, (p_x - i p_y)\beta \} = \Gamma_6 \tag{4.6}$$

$$(J = 3/2, J_z = \pm 1/2) : \{ 2p_z\alpha - (p_x + i p_y)\beta, 2p_z\beta + (p_x - i p_y)\alpha \} \tag{4,7}$$

$$(J = 1/2, J_z = \pm 1/2) : \{ p_z\alpha + (p_x + i p_y)\beta, -p_z\beta + (p_x - i p_y)\alpha \} \tag{4.8}$$

When the three axes (x, y and z) are equivalent (cubic symmetry), the matrix elements of the Hamiltonian between the three p-orbitals are equal. Then one can obtain the eigenfunction of total angular momentum by taking a linear combination of basis functions of two independent Γ_7, that is, from (4.3) and (4.5) to (4.7) and (4.8). However, in the D_{2d} symmetry, the p_z -orbital element is different from the other two. Therefore, in contrast to the fact that the state of the heavy hole remains the eigenfunction of total angular momentum ($J = 3/2, J_z = \pm 3/2$), the light hole state is a mixture of ($J = 3/2, J_z = \pm 1/2$) and ($J = 1/2, J_z = \pm 1/2$) as in the split off band.

It follows that in superlattices the ratio between the light hole oscillator strngth TE-mode (only contributed to by p_x and p_y) and that of TM-mode (only contributed to by p_z) is *not an integer* but has n-dependency. Let us briefly describe some details of the straightforward calculation. The oscillator strength for transitions between valence bands and conduction band minimum at the Γ -point is obtained by calculating

$$\left| \langle c \mid \mathbf{p} \mid v_i \rangle \right|^2 \tag{4.9}$$

where $|c>$ is the wave function of the conduction band minimum and $|v_i>$ is the i-th wave function near the top of valence bands. $\mathbf{p}$ is the momentum operator. In the superlattices, $|c>$ consists of the linear combination of original Ga and As anti bonding s-orbital, and folded states which do not contribute to the oscillator strength. $|v>$'s are the states (4.6) for the heavy hole and linear combinations of the states (4.7) and (4.8), for the light hole and the spin split off band. A typical matrix element of (4.9) becomes

$$\langle c \mid \frac{\partial}{\partial x} \mid v \rangle \tag{4.10}$$

$$= \sum_{l\Gamma i} (a^s_{\Gamma c})^* a^{P_i}_{\Gamma v} \langle S(\mathbf{r}-\mathbf{R}_l) \mid \frac{\partial}{\partial x} \mid P_i(\mathbf{r}-\mathbf{R}_{l'}) \rangle, \tag{4.11}$$

where the coefficient a is obtained by solving the eigenvalue equation and $S(\mathbf{r})$ and $P_i(\mathbf{r})$ ($i = x, y$ and z) are respectively the anti bonding s-orbital and the bonding p-orbitals in a unit cell. The trivially vanishing terms, for instance,

$$\langle P_x(\mathbf{r}) \mid \frac{\partial}{\partial x} \mid P_x(\mathbf{r}) \rangle \tag{4.12}$$

are not written in (4.11). If we employ the approximation of assuming the equality of the matrix elements

$$Q = \langle S(\mathbf{r}) \mid \frac{\partial}{\partial x} \mid P_x(\mathbf{r}) \rangle = \langle S(\mathbf{r}) \mid \frac{\partial}{\partial y} \mid P_y(\mathbf{r}) \rangle \tag{4.13}$$

$$= \langle S(\mathbf{r}) \mid \frac{\partial}{\partial z} \mid P_z(\mathbf{r}) \rangle$$

between the GaAs bond and the AlAs bond in the unit cell and assume all the other *inter-cell* elements to be vanishing, these Q terms cancel when we take a ratio with the oscillator strength in the bulk GaAs case. Thus the ratio of the oscillator strength in superlattices to that of bulk GaAs depends only on the a coefficients of linear combination of atomic orbitals in the ergenfunctions. The calculated results are shown in Fig.4.11 for several combinations of superlattice layer numbers (m, n). In $(GaAs)_2/(AlAs)_2$, although the oscillator strength is not greatly reduced, one can clearly observe the non-integral strength ratio for the light hole, which means the mixing between the two different angular momentum states discussed above is large. For the (3, 3) combination, the reduction of oscillator strength is very great but by increasing the number of layers it gradually recovers the bulk value [See the case of (10, 10) in Fig.4.11(a)]. For contrast with the case of (n, n), let us take an example of (n, 1) , for instance, $(GaAs)_9/(AlAs)_1$ in Fig.4.11(b). The splitting of the heavy hole and the light hole is still considerably large although the calculated TE- and TM- mode mixing ratio in the light hole indicates that the bulk character of the wavefunction is almost completely recovered. This is true for both band offset rules, Kroemer's rule (60% : 40%) and Dingle's, rule (85% ; 15%). However, the splitting is smaller for Dingle's rule becase the splitting between heavy hole and the light hole at the Γ- point is due to the tetragonality of the Bravais lattice in the superlattice which is largely caused by the atomic potential difference between Ga and Al atoms.

These reductions of oscillator strength in the superlattices, especially occuring for small m and n in $(GaAs)_m/(AlAs)_n$, are due to the fact that the wavefunction of the conduction band minimum at the Γ- point consists of the superposition between the original bulk component of the Γ- point (the anti-bonding s-orbital) and the folded states from the states along the Δ-line (or the X-point) of GaAs as well as AlAs. These folded states do not contribute nonvanishing matrix elements of the momentum operator between the

conduction band minimum and the top of valence band. It is briefly shown in the previous paper theat we checked the mixing ratio of the folded states, by comparing the wavefunction with that of the semi-empirical pseudopotential calculation, which is more accurate than the present method. The mixing ratio in $(GaAs)_2/(AlAs)_2$ agreed well with the pseudopotential result of Nakayama and Kamimura.

It should be noted that, strictly speaking, the present discussion has to be understood from the viewpoint of the qualitative comparison between the cases with and without inclusion of spin orbit interaction, because of the restricted meaning of the tight binding method and the approximation employed in the calculation of matrix elements of momentum operator (see the previous paper) . However, this qualitative treatment in the present paper sufficient to show that neither the light hole state nor the spin-split-off band are eigenstates of total angular momentum. It will be desirable to quantify this with a more accurate method of band structure calculation.

Finally, the results of the calculation of energy levels of heavy hole, light hole and the conduction band minimum at the Γ - point are shown in the Fig.4.12 with the result of the Krönig-Penny model calculated by Tokuda.[19]

The parameter values employed by Tokuda are as follows,

	GaAs	AlAs
conduction band effective mass	0.067	0.150
valence band effective mass		
m_{lh}	0.087	0.150
m_{hh}	0.62	0.76

where all values are in the unit of the electron bare mass. The band offset values are chosen according to Kroemer's rule (as in this paper). Note that the heavy hole energy level asymptotically approaches the value for bulk GaAs as does the Krönig-Penny model result but the former is always higher than the latter. This is due to the fact that the role of the energy barrier of AlAs is overestimated in the latter model. The electrons can transfer rather easier than expected. This situation is reflected more strongly in the asymptotic behavior of the light hole. The energy level of the light hole in the Krönig-Penny model is far below that of the present calculation. It is also important to note that in the conduction band the asymptotic behaviors are very different even for $n = 10$. This is due to the fact that in the bulk GaAs the dispersion in the conduction band is very different from the free electron like dispersion assumed in the employment of the free electron band in the Krönig -Penny model.

5 (111) - superlattices

5.1 General properties

As is well known, the zinc blend structure of III-V semiconductor compounds consists of two f.c.c. sublattices which are mutually shifted (1/4, 1/4, 1/4) a, where a is the lattice constant as shown in Fig.5.1. One sublattice is occupied by the III - group element atoms and the other sublattice by the V-group element atoms [20]. When one observes one sublattice from the (111) direction i.e., the configuration of either III - or V - element atoms, one can recognize that there is the three-layer periodic stacking of two-dimensional triangular lattices in the (111) direction [see Fig.5.1].

Now, to determine the primitive unit cell, let us consider the superlattice case of $(III_A\text{-}V_A)_1 / (III_B\text{-}V_A)_1$ which has the same space group symmetry as $(III_A\text{-}V_A)_1 / (III_B\text{-}V_B)_1$ superlattices as we shall show later in this section. The three primitive translation vectors for the atoms of III_A or III_B elements are those

connecting atoms in neighboring layers of triangular lattices as shown in Fig.5.2, so that the resulting Bravais lattice has a rhombohedral structure. The volume of the primitive unit cell is (1/2)a^3, which is twice that of the primitive unit cell of the original zinc blend structure, (1/4)a^3. Necessarily, the new Brillouin zone becomes half of the original f.c.c. Brillouin zone. If one calculates the reciprocal lattice vectors and draws the Brillouin zone for both structures, then one obtains Fig.5.3 and instantly understands that the L - point in the original zinc blend structure is folded to the Γ- point of the new (rhombohedral) zone.

Secondly, let us consider the case of another layer combination, a $(III_A\text{-}V_A)_2$ / $(III_B\text{-}V_A)_1$ superlattice structure. In this case, the primitive translation vector is easily defined by choosing the connecting vectors between the III_B element atoms. In contrast to the first case, the configurational types of the triangular lattices for III_B atoms are all equivalent because the translation period of stacking in the (111) direction is three layers in this case and is equal to the period of the triangular lattices of the f.c.c. structure [see Fig.5.4]. Therefore, the three primitive translation vectors are taken as follows : two are the connecting vectors between the intralayer atoms of the triangular lattices and one is the interlayer connecting vector. Then, the structure of the Bravais lattice is hexagonal, as shown in Fig.5.4. The new Brillouin zone (hexagonal) is drawn in Fig.5.5 with the original f.c.c. zone of the zinc blend structure. One easily observes that 1/3 the way along the (111) line between the Γ- and L - point of the original zone becomes the new zone boundary and 2/3 along the line is equivalent to Γ- point in the new zone.

It is easily understood that these are the only two types of the layer number combinations which give different Bravais lattice structures. Hence, generalizing the above results to the case of $(III_A\text{-}V_A)_m$ / $(III_B\text{-}V_B)_n$, the structures of Bravais lattice are hexagonal for $m+n = 3l$ and rhombohedral for $m+n \neq 3l$, where m, n and l are positive integers.

The point group of the unit cell is C_{3v} for all combinations of m and n. The symmetry of the group C_{3v} is rather lower and this is due to the fact that when observed from the (111) direction, the position of the V element atoms is at the shifted site in the unit cell which is not the high symmetric position and prevents the unit cell from having a symmetry operation such as a horizontal reflection or a rotational reflection (see Fig.5.1, 5.2 and 5.3). This is the reason why, in the consideration of the Bravais lattice, we take, without loss of generality, the rather simple examples of $(III_A\text{-}V_A)_m$ / $(III_B\text{-}V_A)_n$ which have the same V element atoms. Hence, in the determination of the space group of (111) III-V superlattices, it is enough to pay attention to either the III or V element atom configurations which contain different periods.

There are six kinds of space groups belonging to C_{3v} as shown below[18]

156	P3m1	$\Gamma_h\, C_{3v}^1$	$m+n = 3l$
157	P31m	$\Gamma_h\, C_{3v}^2$	
158	P3c1	$\Gamma_h\, C_{3v}^3$	
159	P31c	$\Gamma_h\, C_{3v}^4$	
160	R3m	$\Gamma_{rh}\, C_{3v}^5$	$m+n \neq 3l$
161	R3c	$\Gamma_{rh}\, C_{3v}^6$.	

Four correspond to the hexagonal Bravais lattice and two correspond to the rhombohedral Bravais lattice. Since there are not symmetry operations of either glide plane or screw axis in the present system, one can easily specify the space groups for (111) $(III_A\text{-}V_A)_m$ / $(III_B\text{-}V_B)_n$ superlattices as C_{3v}^1 for $m+n = 3l$ and C_{3v}^5 for $m+n \neq 3l$.

The top of the valence band (Γ- point) of the original zinc blend structure has threefold degeneracy because the eigenstate consists of the three p-like bonding orbitals. In the (111) superlattices, it will split into a few levels due to

the effect of the superlattice crystalline field. Using the group theoretical treatment [18], one can classify the splitting as shown in Table 5.1 for cases both with and without spin orbit interaction. With the inclusion of spin orbit interaction, it should be noted that the top of the valence band splits into three twofold degenerate levels. The basis functions of heavy holes (Γ_4 and Γ_5) indicate that these two levels are degenerate due to time reversal symmetry [18], [21] and are not eigenstates of the total angular momentum. This situation is different from the case of the bulk III-V semiconductors and their (001) superlattices, where the heavy hole state is an eigenstate of the total angular momentum [11], $J = 3/2$ and $J_z = \pm 3/2$. Two irreducible representations of Γ_6 appear and mix together to give the final eigenstates of the light hole and the spin split off band. Thus the same situation as the case of (001) superlattices occurs, that is, the states for the light hole and the split-off band are not eigenstates of the total angular momentum [11]. This will be confirmed when the eigen vectors for each energy level are calculated in the numerical examples in the next section.

5.2 Results of calculation

Fig.5.6 is the resulting band strucuture for bulk GaAs fitted to the pseudopotential calculation. The lowest conduction band fits well but the higher does not, so this band structure should be interpreted to be qualitatively meaningful only as far as the valence bands and the lower part of the conduction bands are concerned.

In Fig.5.7, the calculated band structure is shown for the case without inclusion of spin orbit interaction, along with the folded band structures of bulk GaAs and AlAs, in which the position of the valence band top is shifted by the band offset value calculated according to Kroemer's rule.

The new zone boundary is indicated by (Z) in the rhombohedral Brillouin zone so that one should note that (Z) is equivalent to the midpoint of the line between Γ - and L - points in the original f.c.c. Brillouin zone. The global dispersion of valence bands is similar to that of both bulk materials except new gaps open at the new zone boundary and there is a splitting of degeneracy at the Γ - point.

The present calculation gives the direct gap in the conduction band which is different from the (001) superlattice with the same combination of layers. However, we should not take this result as conclusive because of the qualitative character of the present calculation.

Without inclusion of spin orbit interaction, the top of the valence band splits into two levels obtained in the group theoretical analysis. The result including spin orbit interaction is shown in Fig.5.8. The splitting of the valence band top is also consistent with the result from symmetry considerations. The notation Γ_4 and Γ_5 (the degeneracy due to the time reversal symmetry of the heavy hole state) for the top of the valence band follow that in the ref. 18 but is different from that in the ref. 22. As noted in §5.1 the eigenfunctions of these two states are not the eigenstates of the total angular momentum. This fact is different from the case of (001) superlattices, where the heavy hole state is the eigenstate of the total angular momentum. The detailed description of the eigenstate for (001) superlattiecs is given in the other paper*.

The eigenfunctions of the light hole and the spin split-off band consists of the superposition of two Γ_6 - states. Each of the Γ_6 - states is an eigenstate of the total angular momentum $J = 3/2, Jz = \pm 1/2$ ($|3/2, \pm 1/2\rangle$) and $J = 1/2, Jz = \pm 1/2$ ($|1/2, \pm 1/2\rangle$), so that the superposition of these two states gives the non-

---

* S.Nara : preprint

---

integer ratio between the optical polarization (TE- and TM- mode) in the absorption spectrum of these two levels. The coefficient of superposition depends on the band offset value. Therefore, the precise measurement of this ratio allows the determination of the band offset value experimentally, which is independent of the other methods of measuring the band offset value. It is desirable that detailed observation of the optical polarization in the (111) superlattices as well as in the (001) superlattices of III - V semiconductor compounds is performed.

6 Concluding remarks

In this report, the electronic band structures of microscopic superlatteces are discussed, especially, in GaAs - AlAs systems using an improved tight binding method developed by the present author. In both (100) and (111) superlattices, band dispersion are delicately different depending on the selectin of band offset values. At the top of valence band, the electronic states have a large number of variation due to the combination between the spin - orbit interaction and the crystelline field of tetragonal or trigonal symmetry which is caused by forming the (100) or (111) superlattices. They appears as the polarization anomaly in the optical properties as absorption or emission of light.

It is desirable to investigates semiconductor superlattices theoretically and experimentally since they have many possibilities as a one of key materials to realize electronically and optically new functional devices in future.

Referencs

1) L. Esaki and R. Tsu : IBM Journal of Research and Development 14 (1970) 61.

2) R.Dingle : Advances in Solid State Physics, Vol.15. Festkörperprobleme, ed. H. J. Queisser (Pergamon Vieweg 1975)

3) T. Ando, A. B. Fowler and F. Stern : Rev. Mod. Phys. 54 (1982) 437

4) N. Hamada, S. Ohnishi and A. Oshiyama : *Extended Abstracts of the 18the Int. Conf. Solid State Devices & Materials* (business Center for Academic Societies, Jpn, Tokyo, 1986) p.343, N. Hamada and S. Ohnishi : Superlattices and Microstrucuters 3, No. 3 (1987) 301

5) T. Nakayama and H. Kamimura : J. Phys. Soc. Jpn. 54 (1982) 4726, T. Nakayama and H. Kamimura :. *Proc. 18th Int. Conf. Semiconductor Physics* (Stockholm, 1986)

6) E. Yamaguchi : to be published in Jpn. J. Appl. Phys.

7) J. N. Shulman and T. C. McGill : J. Vac. Sci. & Technol. 15 (1978) 815, J. N. Shulman and T. C. McGill : Phys. Rev. B19 (1979) 6341, J. N. Schulman and Yia-Chung Chang : Phys. Rev. B33 (1986) 2594, Ed Caruthers and P. J. Lin-Chung : Phys. Rev. B17 (1978) 2705, W. Andreoni and R. Car : Phys. Rev. B15 (1980) 3334

8) G. C. Osbourn : J. Appl. Phys. 53 (1982) 1586.

9) A. Oshiyama and M. Saito : to be appeared in Phys. Rev. B

10) Bylander and Kleinman, Phys. Rev. B34 (1986) 5280.

11) S. Nara : Jpn. J. Appl. Phys. 26 (1987) 690, S. Nara : Jpn. J. Appl. Phys. 26 (1987) 690, S. Nara : to be published in Jpn. J. Appl. Phys. 26 (1987) No.10, S. Nara : to be published in the *Proc. Int. Symp. on the Technology for Optoelectronics* (Cannes, France, 1987) ; " *Quantum Wells and Superlattices in Optoelectronic Devices and Integrated Optics* " ed. A. R. Adams (SPIE-The Int. Soc. Opt. Eng., Bellingham, Washington, 1988)

12) J. R. Chelikowsky and M. L. Cohen : Phys. Rev. B14 (1976) 556.

13)*Solid State Physics*, 24 eds. F. Seitz and D. Turnbull (Academic Press, New York and London, 1970).

14)P. O. Löwdin : J. Chem. Phys. 18 (1950) 365.

15)H. Kroemer : Proc. the Yamada Conf. VII on Modulated Semiconductor Structures ed. H. Sakaki Surf. Sci 174 (1986).

16)J. C. Slater and G. F. Koster : Phys. Rev. 94 (1954) 1498.

17) L. I. Schiff : *Quantum Mechanics*, (McGrawhill, 1955)

18) C. J. Bradley & A. P. Cracknell : *The Mathematical Theory of Symmetry in Solids*, (Clarendon Press Oxford 1972).

19) K. Tokuda : private communination.

20) R. W. G. Wyckoff : *Crystal Structure* [Interscience Publishers (a division of John wiley & Sons), New York London Tronto 1965]

21) Y. Onodera and M. Okazaki : J. Phys. Soc. Jn. 21 (1966) 2400

22) C. Mailhiot and D. L. Smith : Phys. Rev. B35 (1987) 1242

Figure Captions

Fig.1.1 The resulting fitted band structure of bulk GaAs to the pseudopotential calculation.the present calculation ———, the ref. 11 - - - -

Fig.4.1 The Brillouin zone of zinc blend (- - - -) and simple tetragonal (———)structures which is representatively realized in the bulk GaAs and the$(GaAs)_1/(AlAs)_1$ superlattece, respectively.

Fig.4.2 (a) The unit cell of the $(GaAs)_2/(AlAs)_1$ superlattice with its primitive translation vectors and (b) the corresponding Brillouin zone. In the former, the indication of positions of As is omitted to avoid the complcated description.

Fig.4.3 The calculated band dispersion of $(GaAs)_3/(AlAs)_1$ in the extended zone scheme with the bulk band of GaAs for comparison.

Fig.4.4 (a) The calculated band dispersion of $(GaAs)_4/(AlAs)_1$ and (b) of $(GaAs)_1/(AlAs)_4$, both in the extended zone scheme. Compare with the bulk band structures of GaAs or AlAs.

Fig.4.5 The calculated result for $(GaAs)_1/(AlAs)_9$ in the extended zone scheme, where the scale of the vertical axis is enlarged since the two dimensional character of electronic state becomes stronger for increasing n and.the dispersion becomes flat more and more.

Fig.4.6 The band gap alternation depending on n in $(GaAs)_n/(AlAs)_1$ (a) and $(GaAs)_1/(AlAs)_n$ (b).

Fig.4.7 The extended Brillouin zone for zinc blend and tetragonal strctures.

Fig.4.8 The ocsillator strength dependencies on n for $(GaAs)_n/(AlAs)_1$ (a) and $(GaAs)_1/(AlAs)_n$ (b).

Fig.4.9 The valenceband structure of $(GaAs)_1/(AlAs)_1$ with inclusion of spin-orbit interaction. Each level is two fold degenerate. Note the

degeneracy of the heavy hole and the light hole at the Γ - point in the bulk GaAs is split.

Fig.4.10 The comparison between the detailed band dispersions to the (001) direction near the top of valence band. The notation HH and LH means the heavy hole and the light hole. The thick solid line (———) is the superlattice $(GaAs)_1/(AlAs)_1$, denoted by SL, *with* the spin-orbit interaction. The thin solid line (———) is the $(GaAs)_1/(AlAs)_1$ *without* the spin-orbit interaction, where the type of *p*-orbital wavefunctions at the valenceband top is shown as p_x, p_y and p_z. The broken line (--------) is the *bulk* GaAs *with* the spin-orbit interaction, where the eigenstates of total angularmomentum at the top of valence band are indicated as (J, J_z).

Fig.4.11 (a) The n dependence of the oscillator strength for the heavy hole (the solid line) and the ligth hole (the broken line) in $(GaAs)_n/(AlAs)_n$. The vertical axis is normalized by the oscillator strength ($| < c | -ih\partial/\partial x | p_x > |^2$) of bulk GaAs. (b) The oscillator stength of $(GaAs)_9/(AlAs)_1$ for the band offset values based on Kroemer's rule (solid line) and Dingle's rule (broken line). The normalization of the vertical axis is the same as that of Fig.4.11(a).HH and LH denote the heavy hole and the light hole respectively.

Fig.4.12 (a) The n dependence of valence band edge for the heavy hole (HH) and the light hole (LH), described by the upper curve and the lower curve respectively for both $(GaAs)_n/(AlAs)_n$ and $(GaAs)_n/(AlAs)_1$. For comparison, the results based on the Krönig-Penny model calculated by Tokuda are shown. The values of parameters used in Tokuda's calculation are listed in the paper. In the Krönig-Penny model the width of each layer is a continuous valued variable so that the layer number n (integer) is replaced by d in the figure. (b) The n dependence of the two lower conduction band edge at the Γ - point for

both $(GaAs)_n/(AlAs)_n$ (the solid line) and $(GaAs)_n/(AlAs)_1$ (the broken line). As in the (a), the results obtained by Tokuda based on the Krönig-Penny model are shown for comparison.

Fig.5.1 The unit cell of the zinc blend structure, where the body diagonal direction is taken as a vertical direction. The closed circle represents the III - element atoms and the cross mark the V - element atoms. Note that the triangular lattices are stacked in the vertical (body diagonal) direction with a period of three layers. The primitive translation vectors are represented by arrows and the symmetry of the Bravais lattice is f.c.c..

Fig.5.2 The unit cell of the (111) superlattice of $(III_A\text{-}V_A)_1 / (III_B\text{-}V_A)_1$. The closed circles represent the III_A - element atoms and the open circles arethe III_B- atoms. The cross mark is the V_A - atoms. Note that the primitive translation vectors are represented by arrows and the symmetry of the Bravais lattice is rhombohedral. The volume of the unit cell is twice the volume of the f.c.c. unit cell shown in Fig.5.1(a).

Fig.5.3 The first Brillouin zone of the rhombohedral Bravais lattice and the Brillouin zone of the (111) superlattice, $(III_A\text{-}V_A)_1 / (III_B\text{-}V_A)_1$, is drawn with the original f.c.c. zone of the zinc blend structure. Note that the mid point of the line from Γ to L in the original f.c.c. structure becomes the new zone boundary, so that the L - point is folded to the Γ - point in the superlattice structure.

Fig.5.4 The unit cell of the (111) superlattice of $(III_A\text{-}V_A)_2 / (III_B\text{-}V_A)_1$. The meaning of the symbols is the same as those of Fig.5.1 and Fig.5.2. In the lower half, only the atomic configuration of III-element atoms is shown to avoid complexity of figure. Note that the broken line arrows are the primitive translation vectors of f.c.c. structure if all points are equivalent and the solid line arrows are the primitive translation vectors of the hexagonal lattice of the present superlattices. In the

lower half, the atomic positions of V - element atoms are put into the figure and the solid line frame indicates the equivalent unit cell which is drawn in order to show the symmetry of this type of superlattice.

Fig.5.5 The first Brillouin zone of the present (hexagonal) (111) superlattice of $(III_A\text{-}V_A)_2 / (III_B\text{-}V_A)_1$. Note that 1/3 the way along the (111) line (Γ to L) is the zone boundary of new structure, so that 2/3 along the line becomes equivalent to the Γ - point.

Fig.5.6 The band structure of bulk GaAs fitted to the pseudopotential calculation by M. L. Cohen et al. Note that the lowest conduction band is well reproduced.

Fig.5.7 The calculated band structure of (111) superlattice, $(GaAs)_1/(AlAs)_1$ with the band structure of bulk GaAs and AlAs which is folded about the midpoint of the line from Γ to L . Spin-orbit interaction is not included. Note that new gaps open at the new zone boundary and the top of valence band splits into two levels as predected by the group theoretical treatment.

Fig.5.8 The same as Fig.5.5 with the inclusion of spin orbit interaction. The band structure near the top of the valence band is shown. For comparison, the dispersion of bulk GaAs is shown by the broken line.

NARA 1/2 Fig. 1.

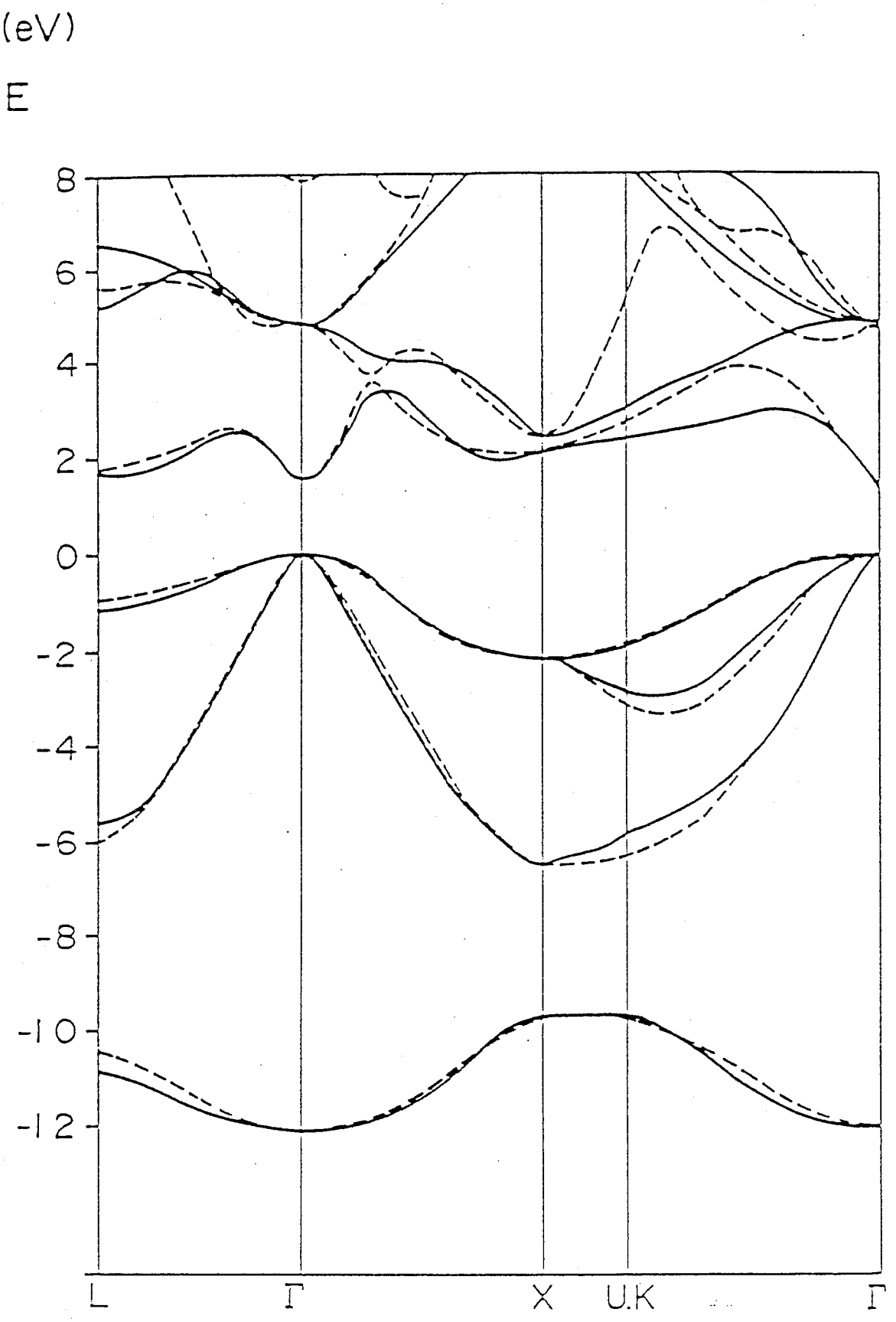

NASA

Fig 4.1

1/2

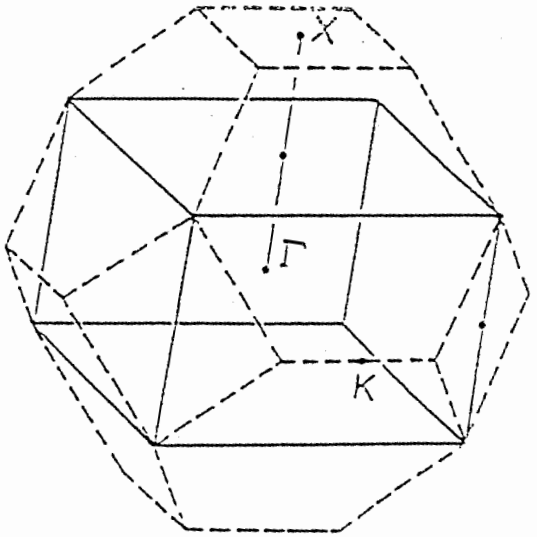

1/2

○ Al

● Ga

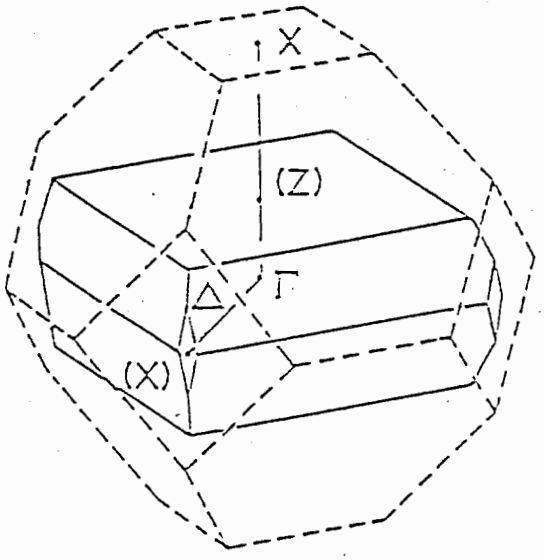

Fig 4.2 (b)

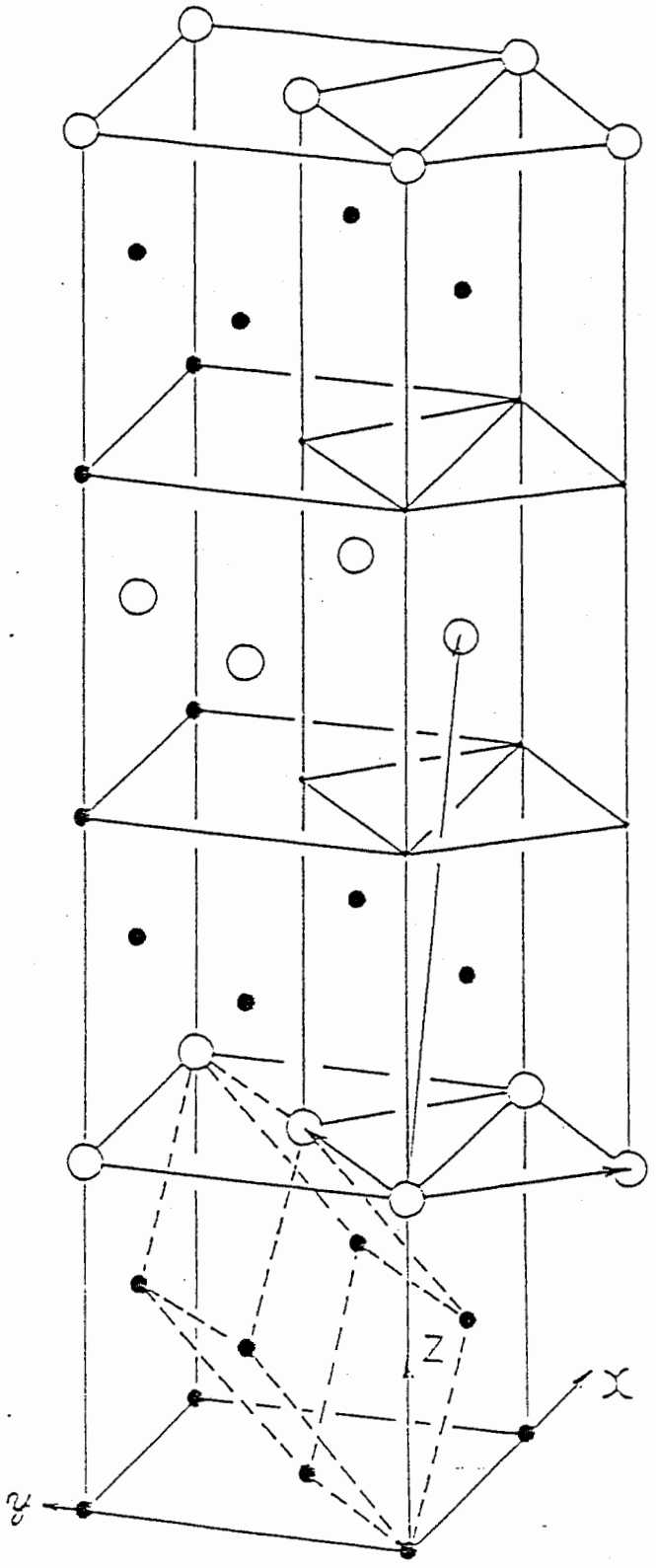

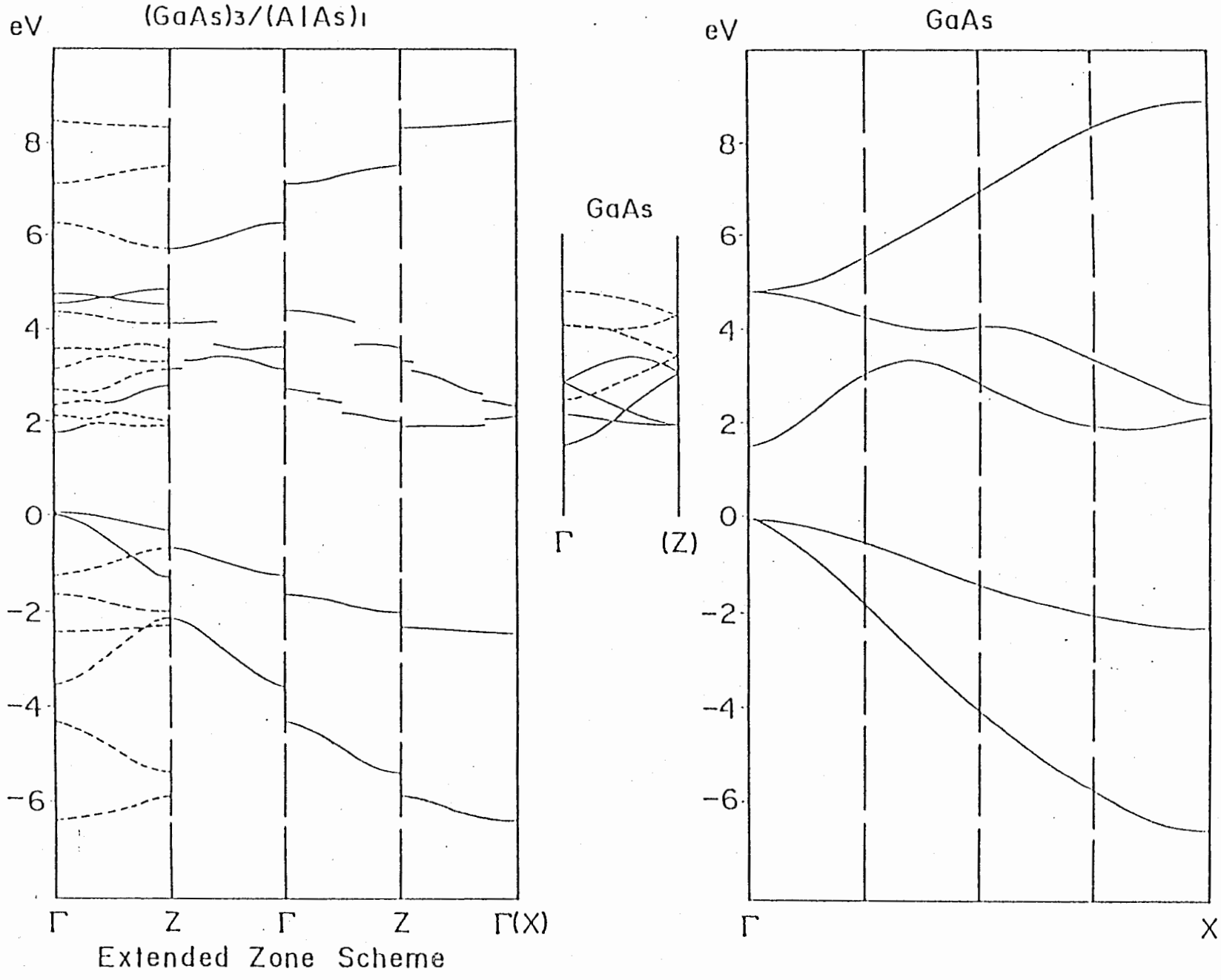
eV
(GaAs)3/(AlAs)1
8
6
4
2
0
-2
-4
-6
Γ
Z
Γ
Z
Γ(X)
Extended Zone Scheme
GaAs
Γ
(Z)
eV
GaAs
8
6
4
2
0
-2
-4
-6
Γ
X

Fig. 4.4 (a) (8.5)

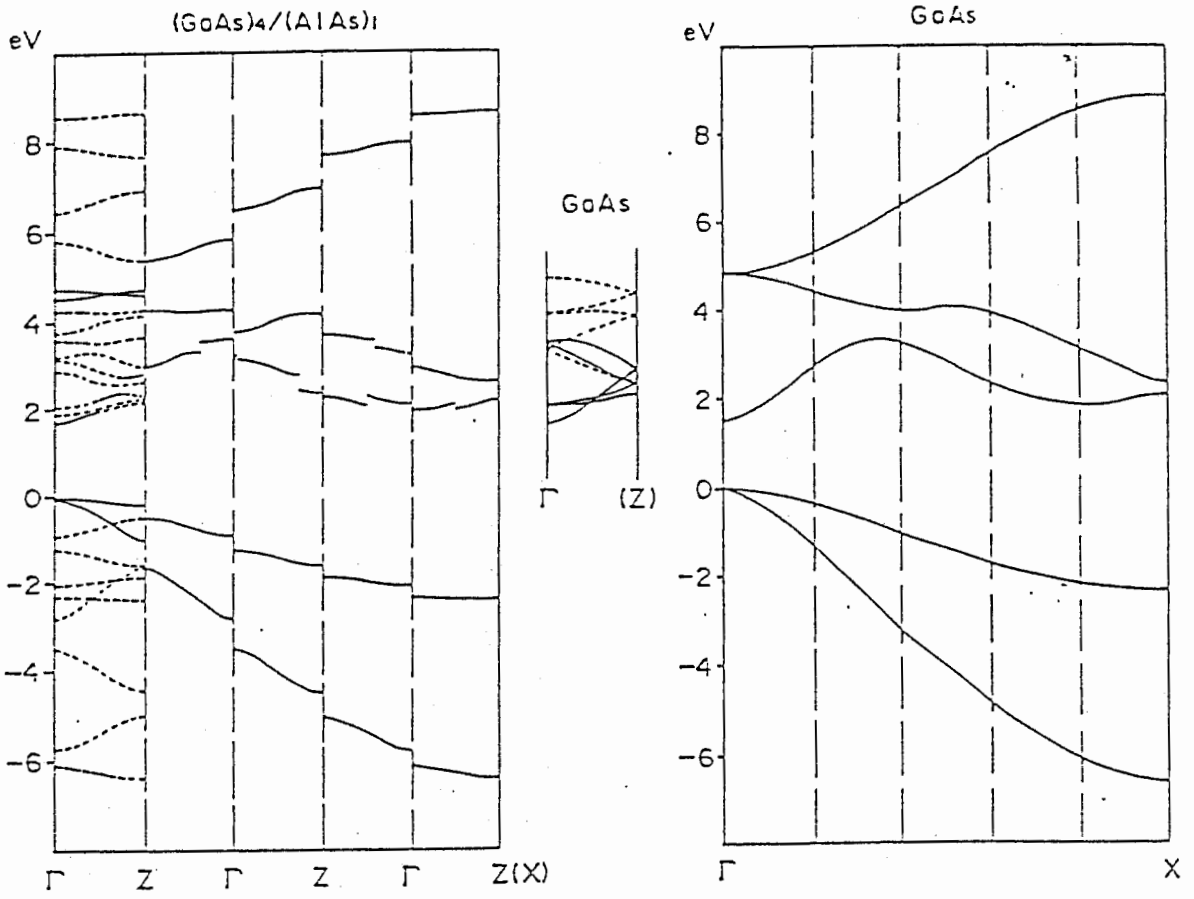

Fig. 4.4 (b)

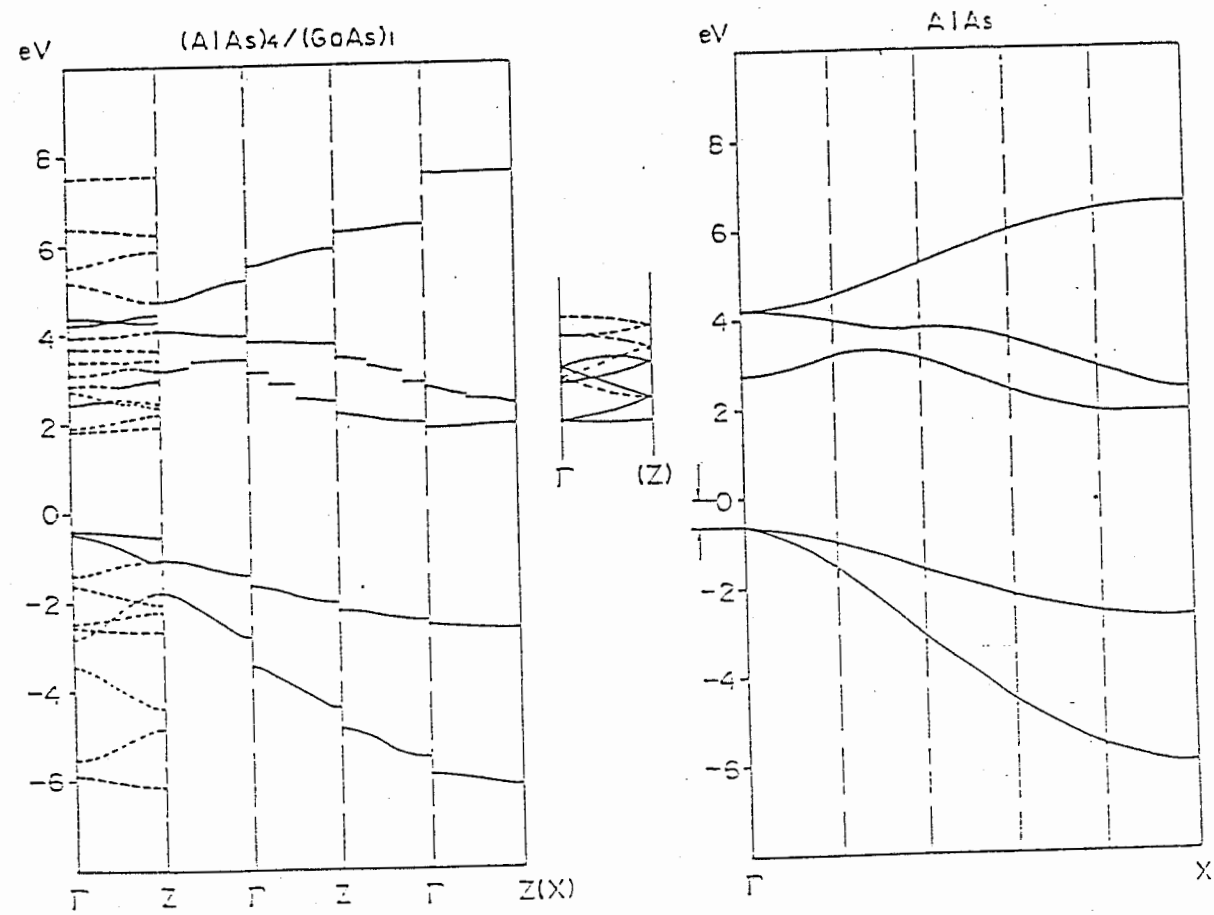

10 99

AlAs
eV
8
6
4
2
0
-2
-4
-6
X
Γ(Z)
AlAs
Γ
Z
(GaAs)1/(AlAs)9
eV
4
3
2
1
0
-1
-2
-3
-4
Γ
Z
Γ
Z

Fig. 4(a)

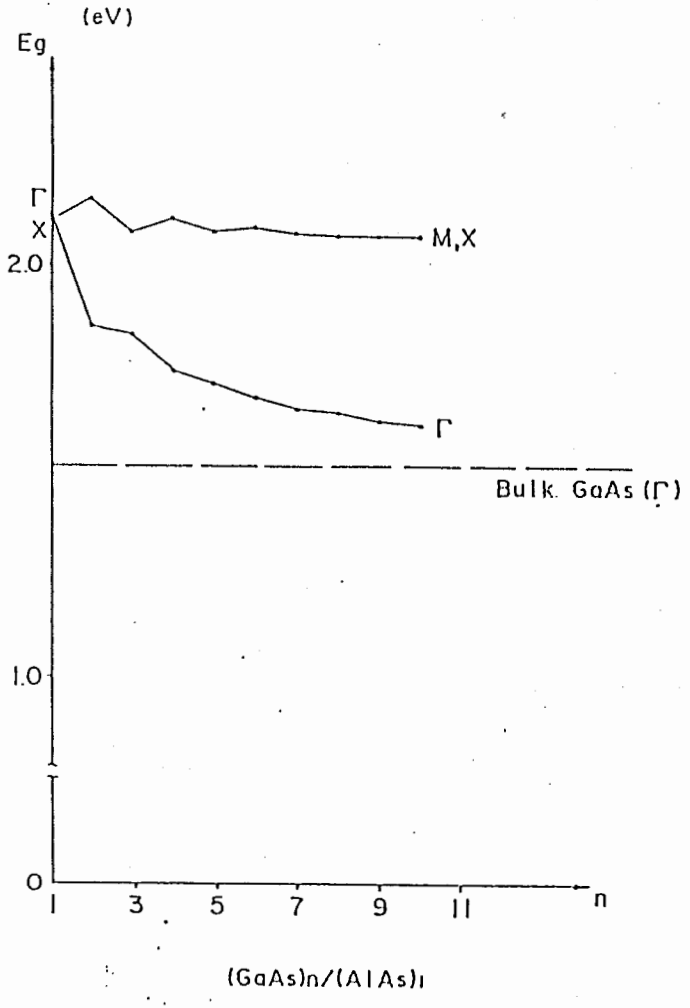

73%

NARA

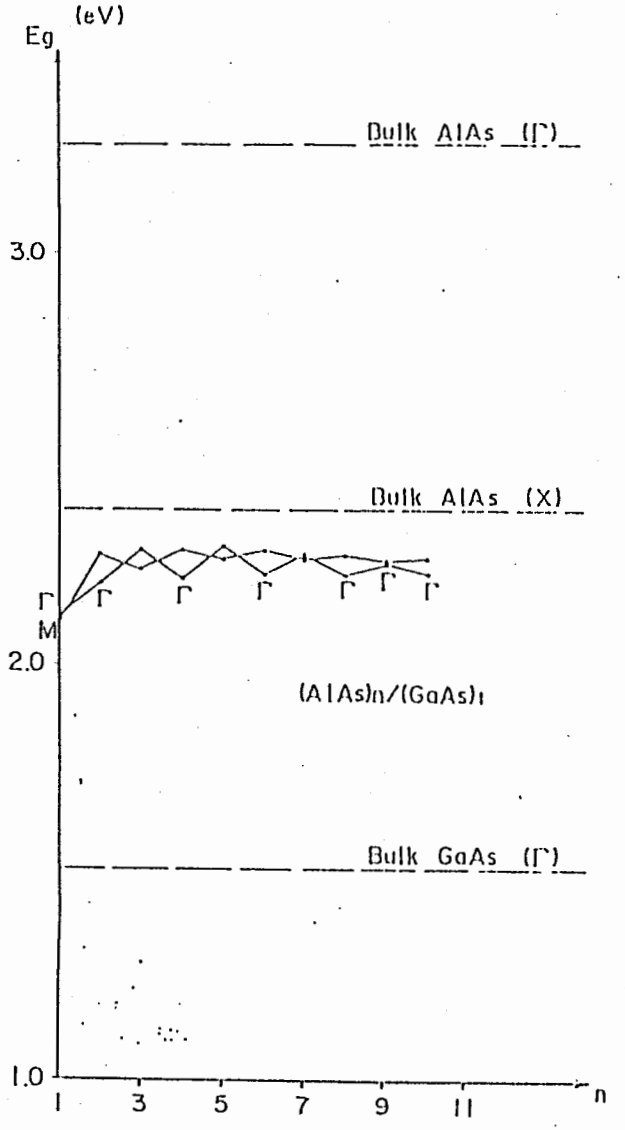

73%

(V2)

NARA

Fig. 4.7

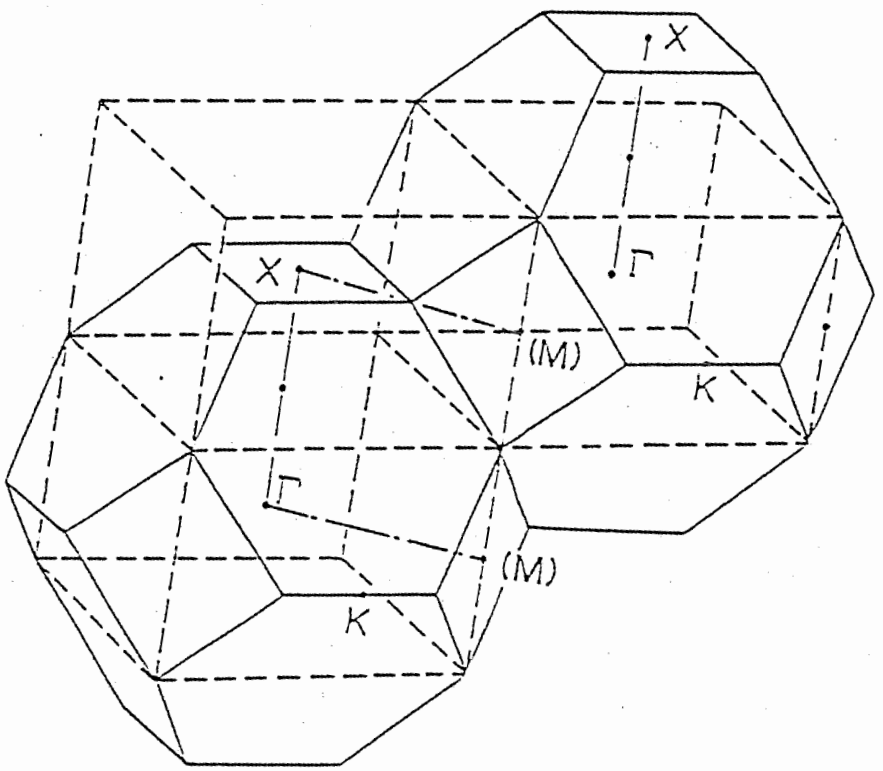

Fig. 4.8(a)

NARA

Fig. 4.8(b)

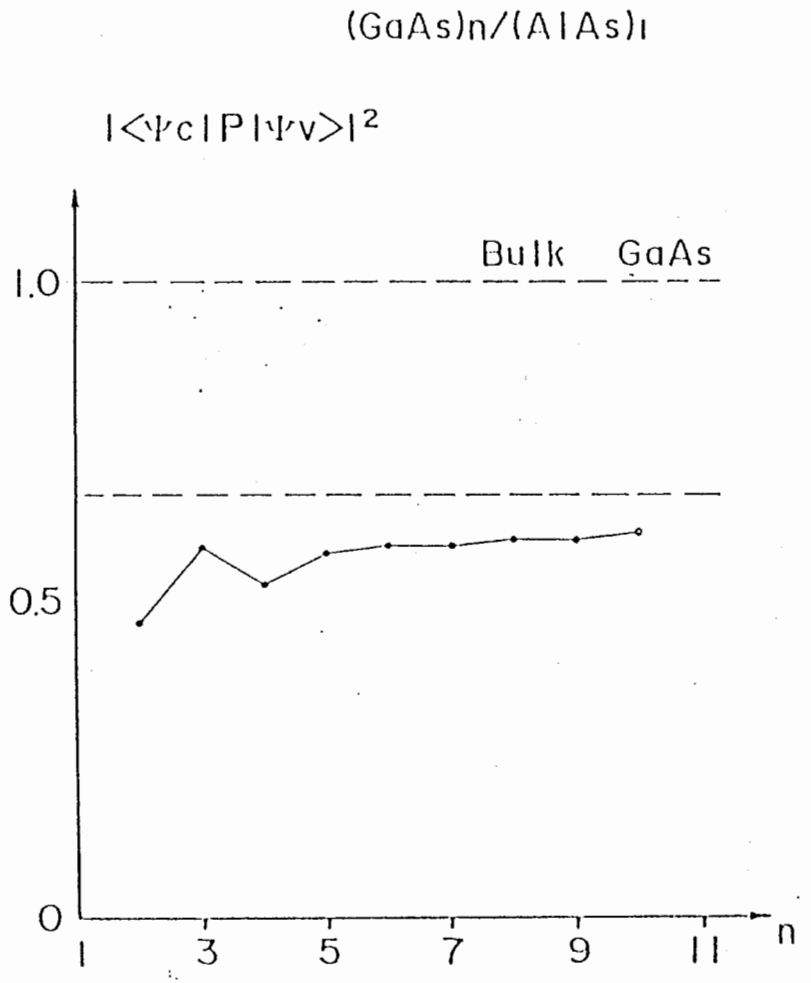

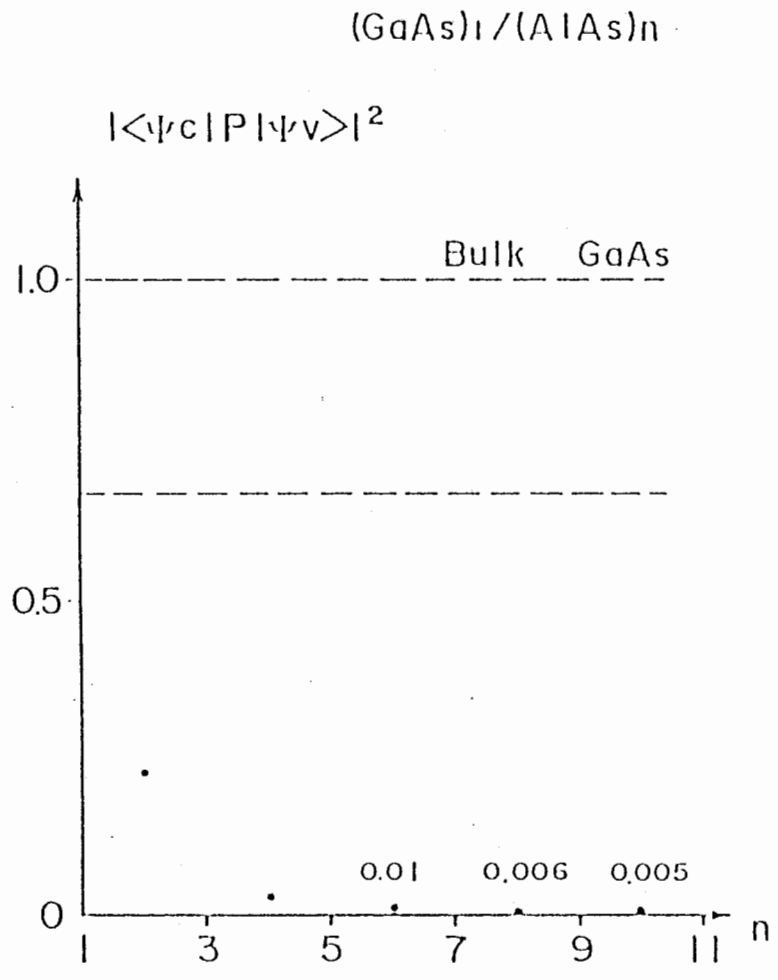

Fig. 4.9

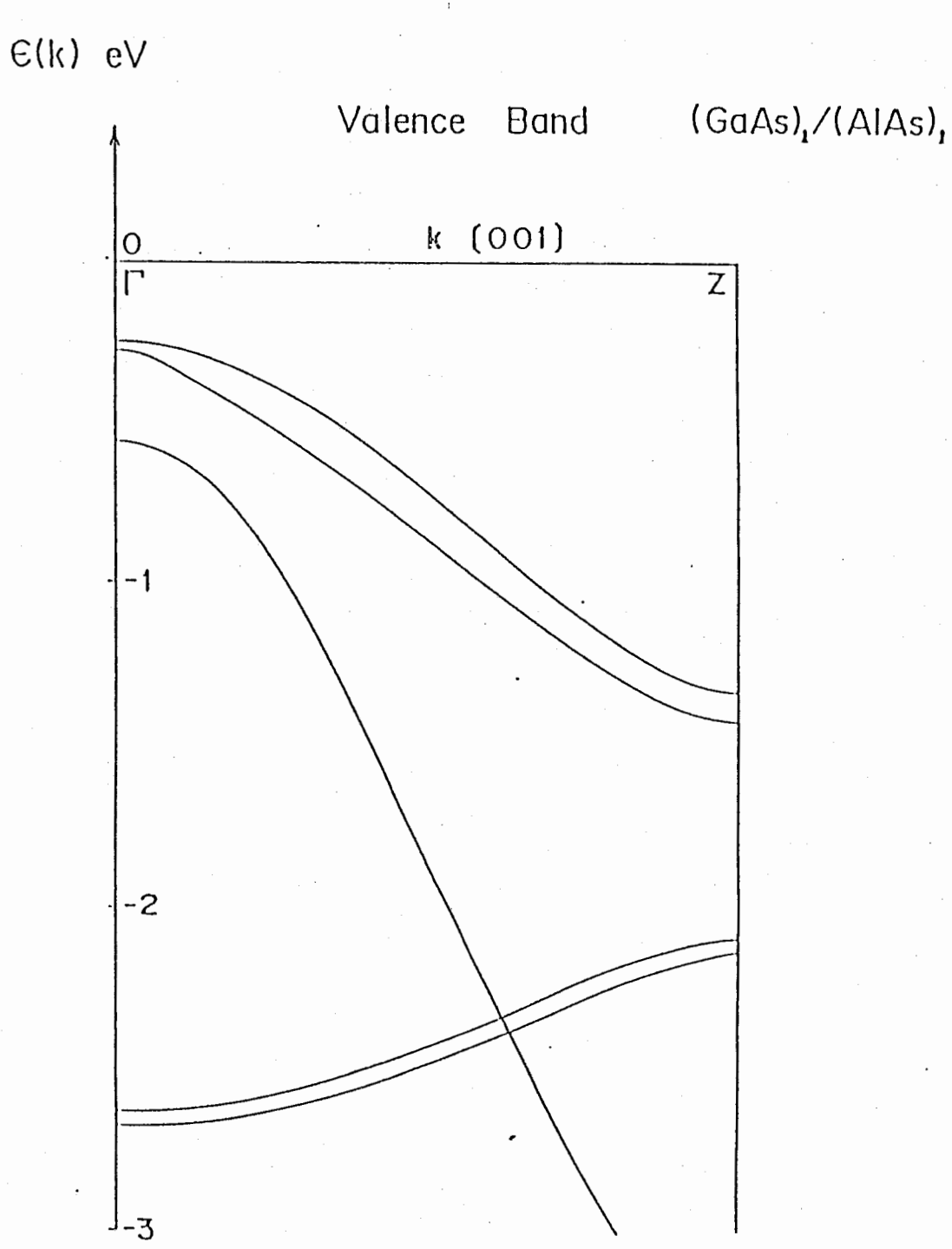

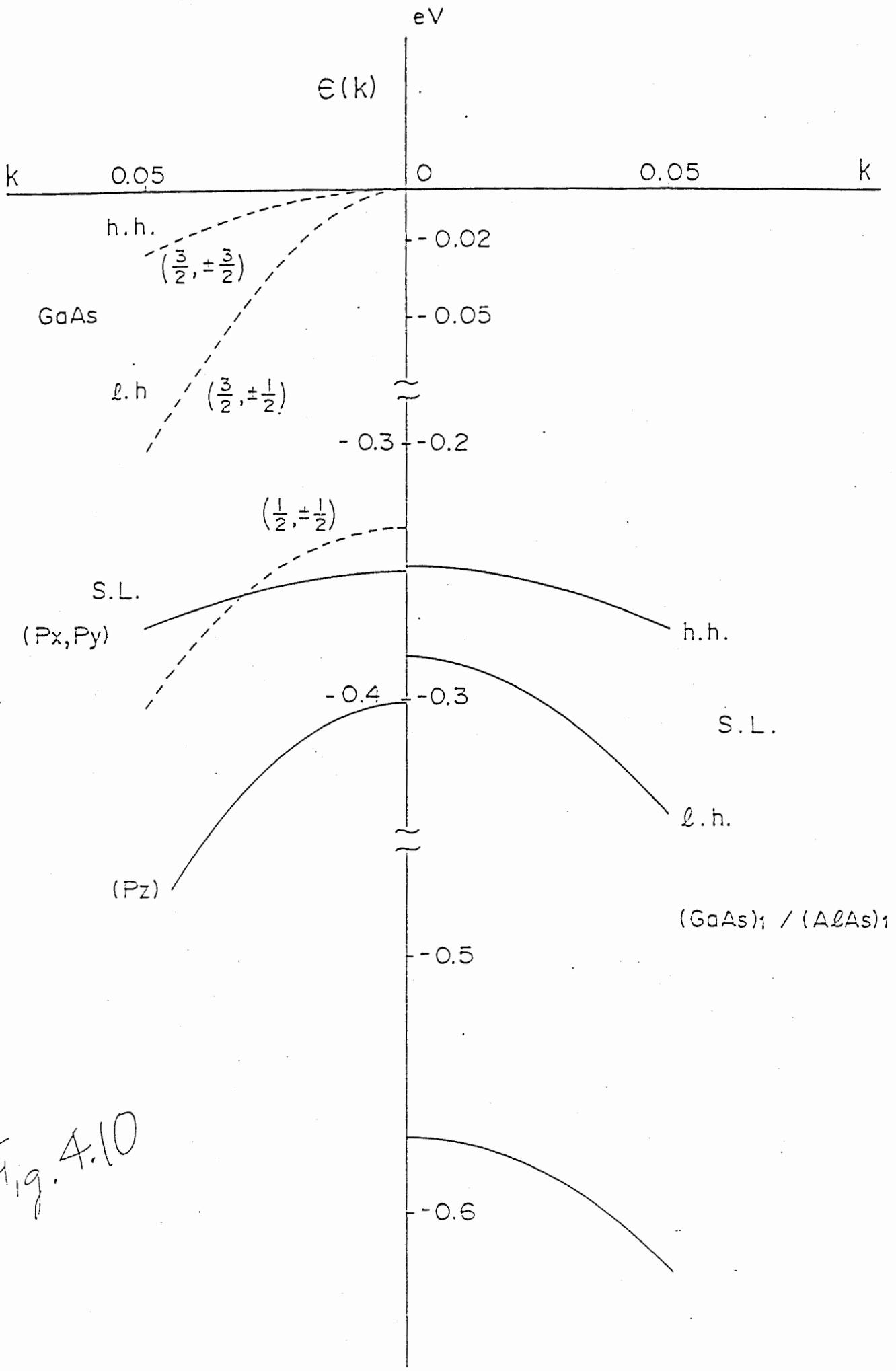
eV
$\epsilon(k)$
k
0.05
0
0.05
k
h.h.
$(\frac{3}{2}, \pm\frac{3}{2})$
GaAs
ℓ.h
$(\frac{3}{2}, \pm\frac{1}{2})$
$(\frac{1}{2}, \pm\frac{1}{2})$
S.L.
(Px, Py)
h.h.
S.L.
ℓ.h.
(Pz)
$(GaAs)_1 / (A\ell As)_1$
- 0.02
- 0.05
- 0.3
- 0.2
- 0.4
- 0.3
- 0.5
- 0.6

Fig. 4.10

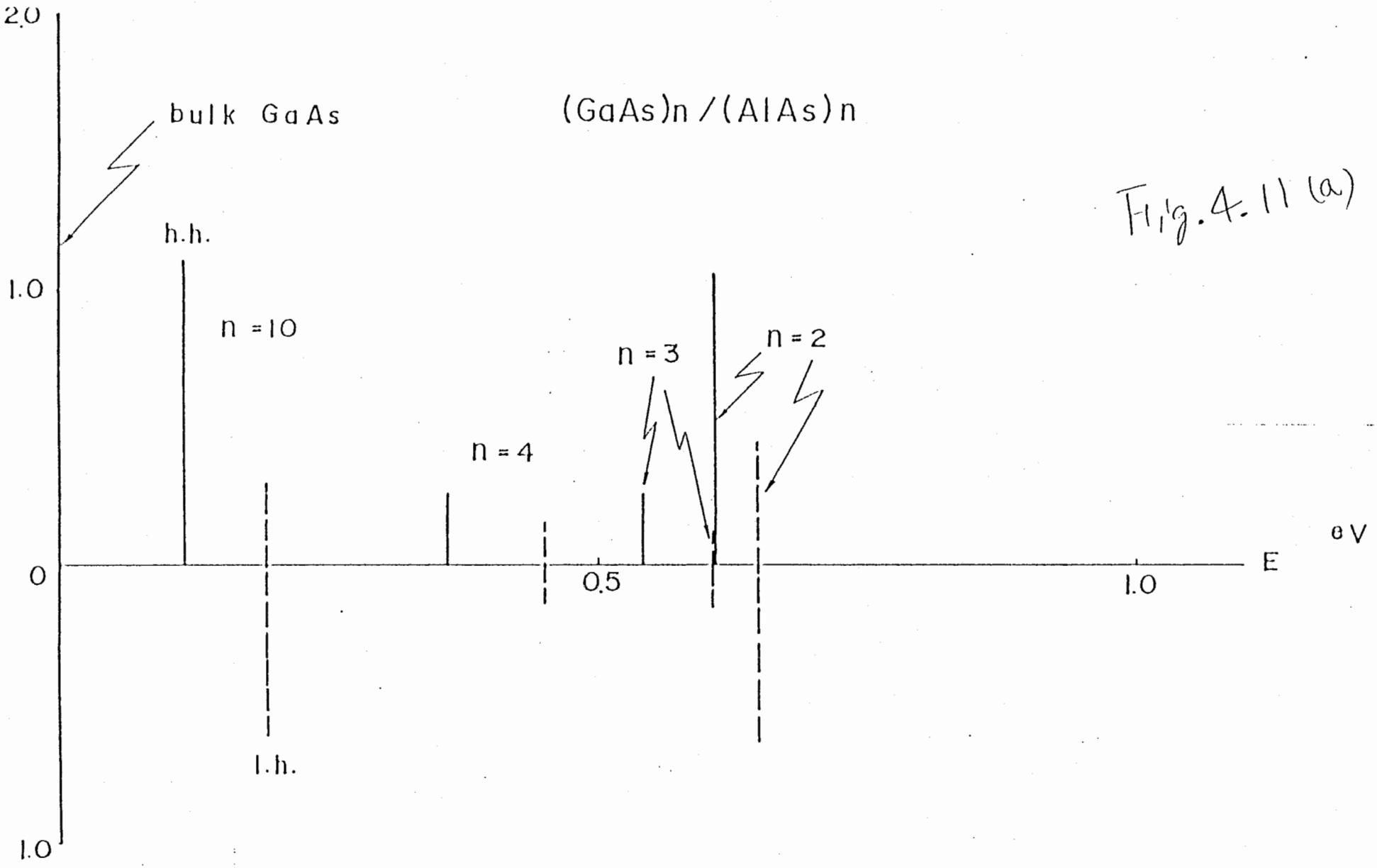

Fig. 4.11 (a)

TM

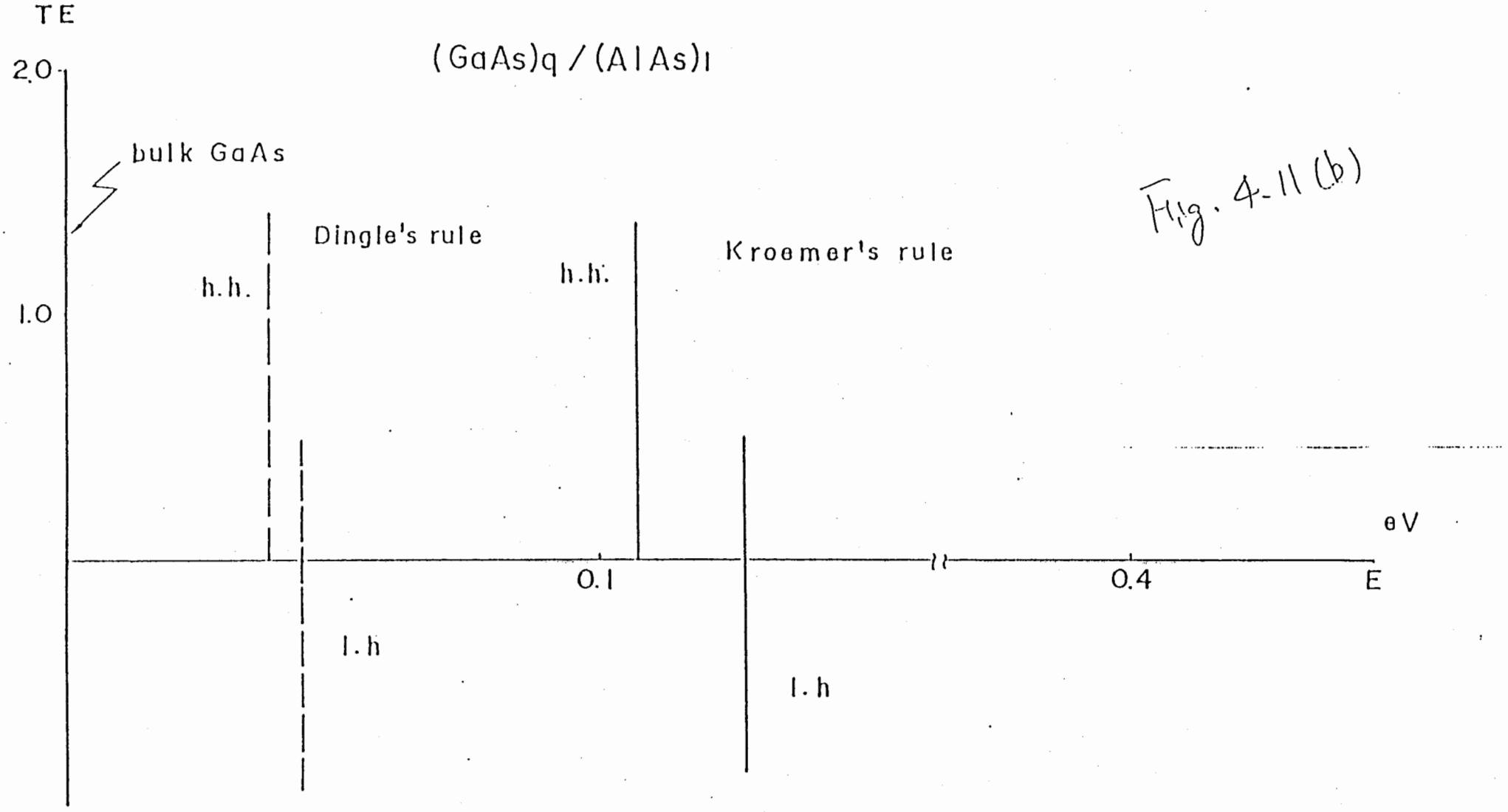
TE
(GaAs)q / (AlAs)l
2.0
1.0
bulk GaAs
h.h.
Dingle's rule
h.h.
Kroemer's rule
eV
0.1
0.4
E
l.h
l.h
TM

Fig. 4-11 (b)

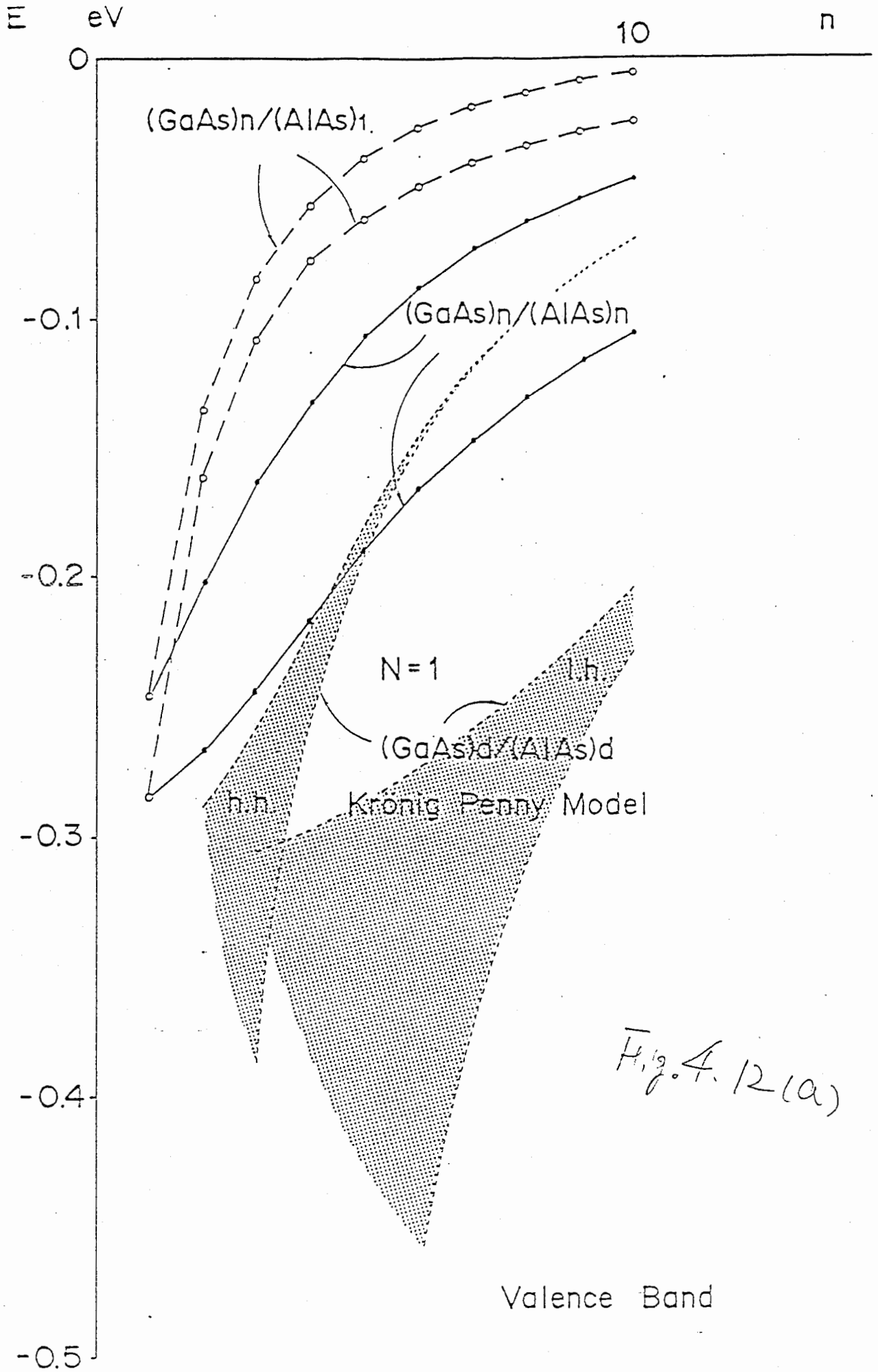
E eV
10
n
0
-0.1
-0.2
-0.3
-0.4
-0.5
(GaAs)n/(AlAs)1
(GaAs)n/(AlAs)n
N=1
l.h.
(GaAs)d/(AlAs)d
h.h
Kronig Penny Model
Valence Band

Fig. 4.12(a)

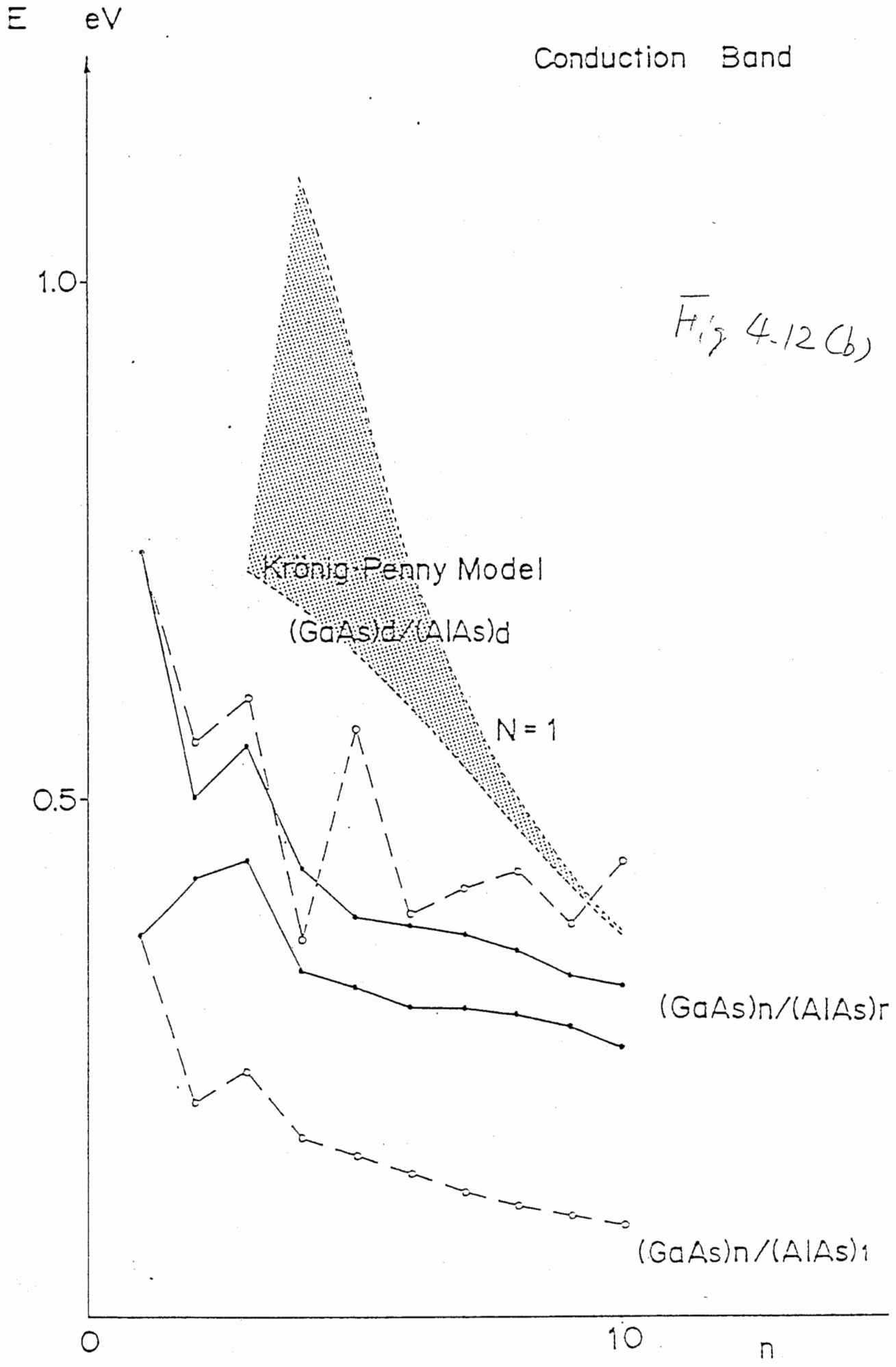
E eV
Conduction Band
1.0
0.5
Kronig-Penny Model
(GaAs)d/(AlAs)d
N = 1
(GaAs)n/(AlAs)r
(GaAs)n/(AlAs)1
0
10
n

Fig 4.12 (b)

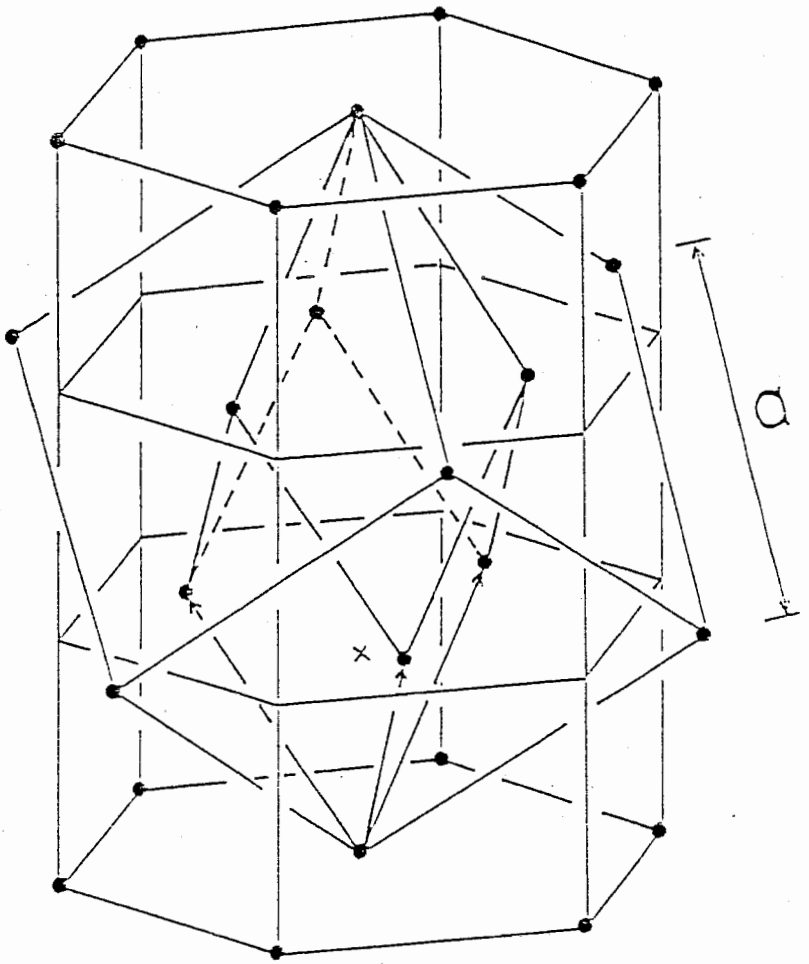

Fig. 5.1

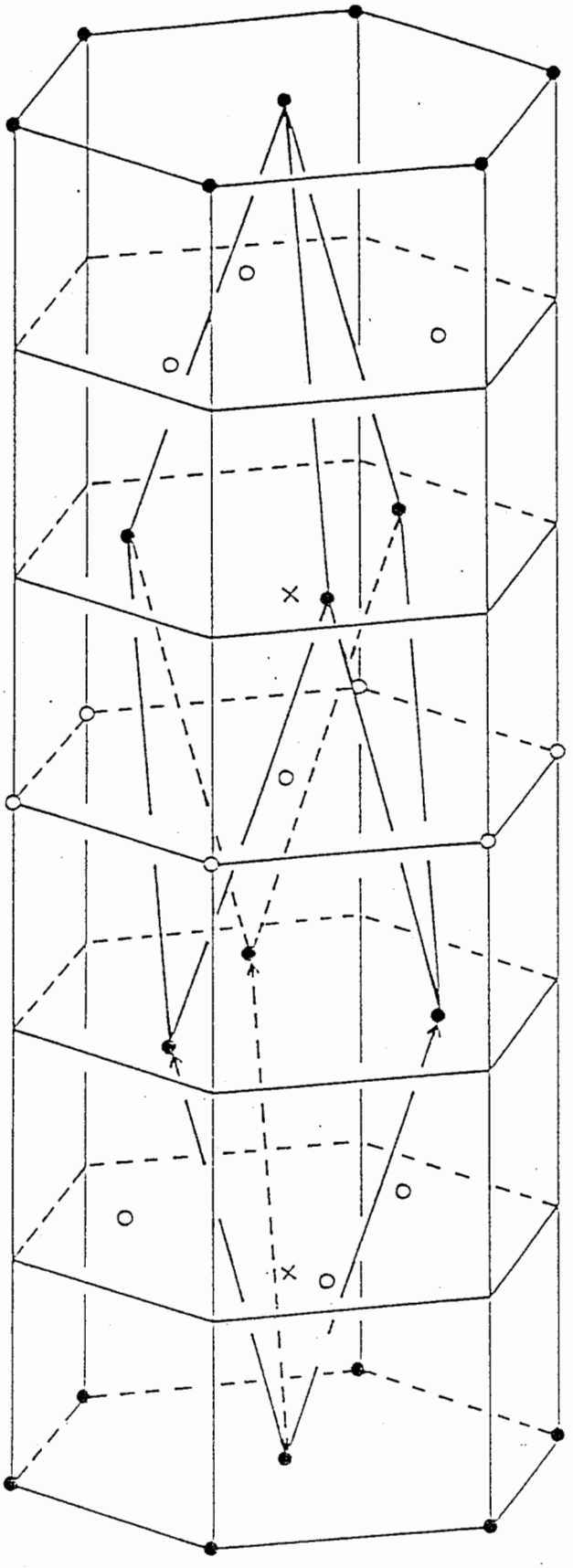

Fig. 5.2

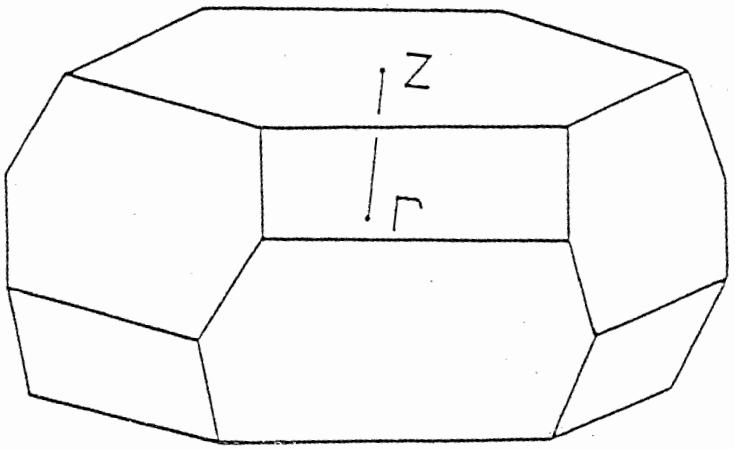

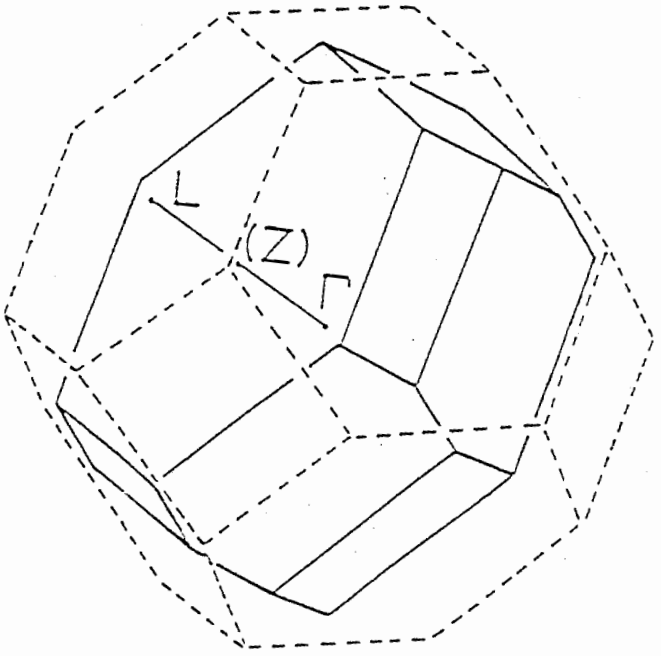

Fig. 5.3

Fig. 5.4

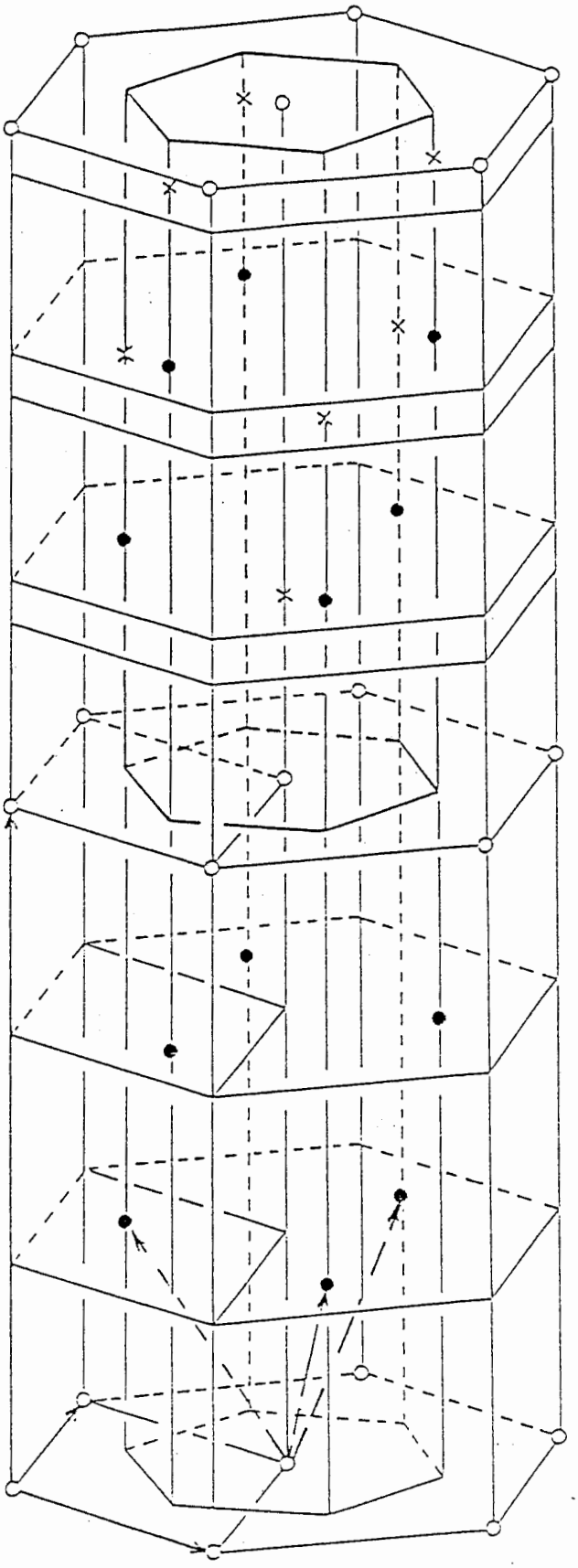

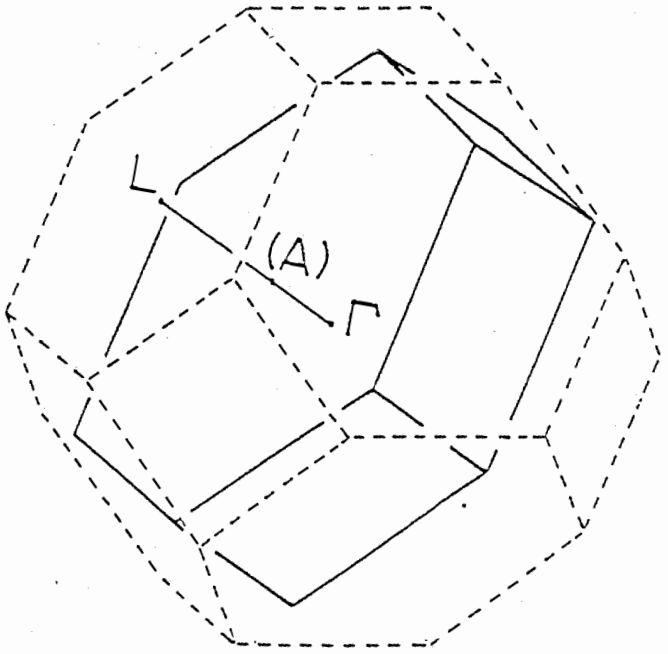

Fig. 5.5

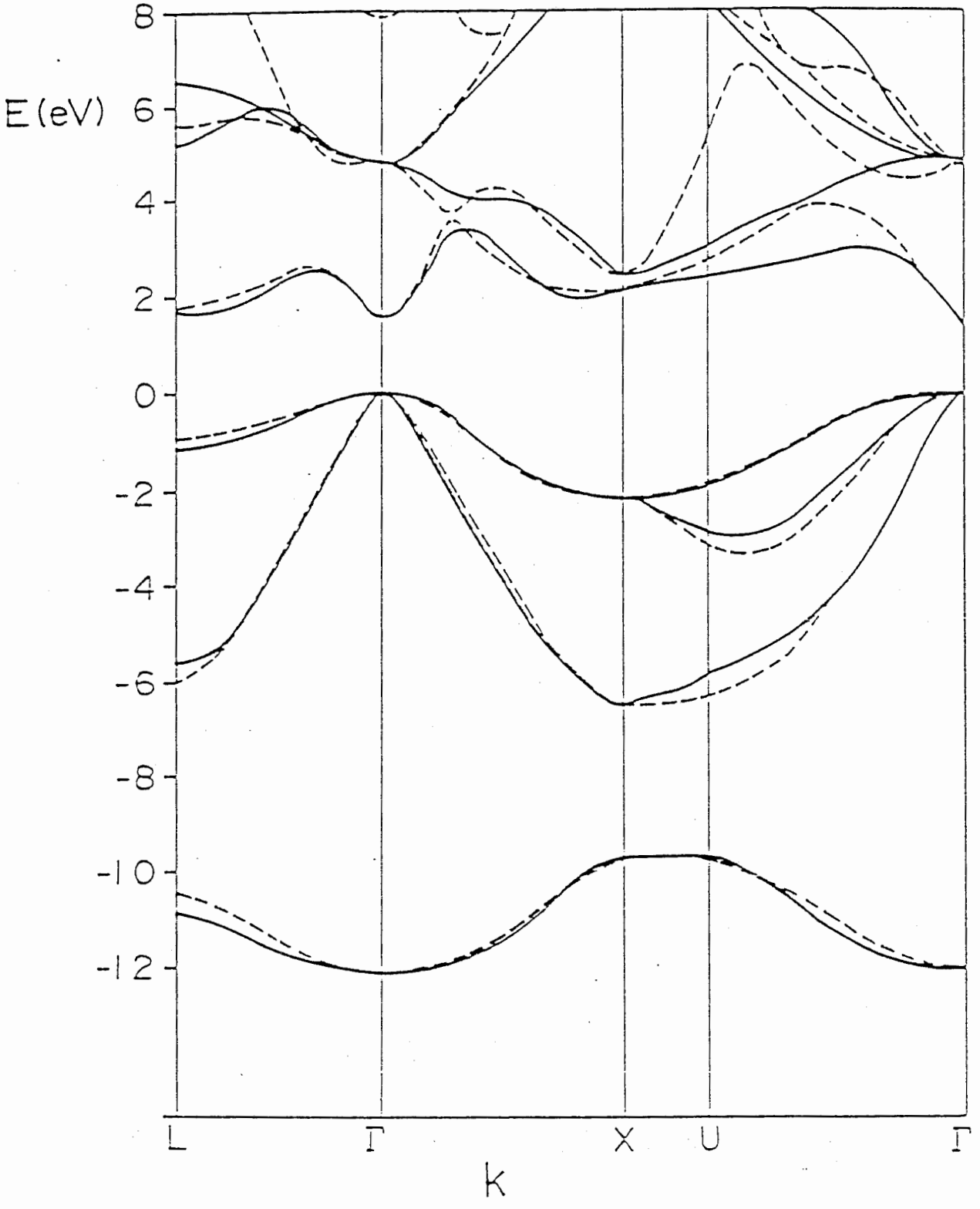

Fig. 5.1

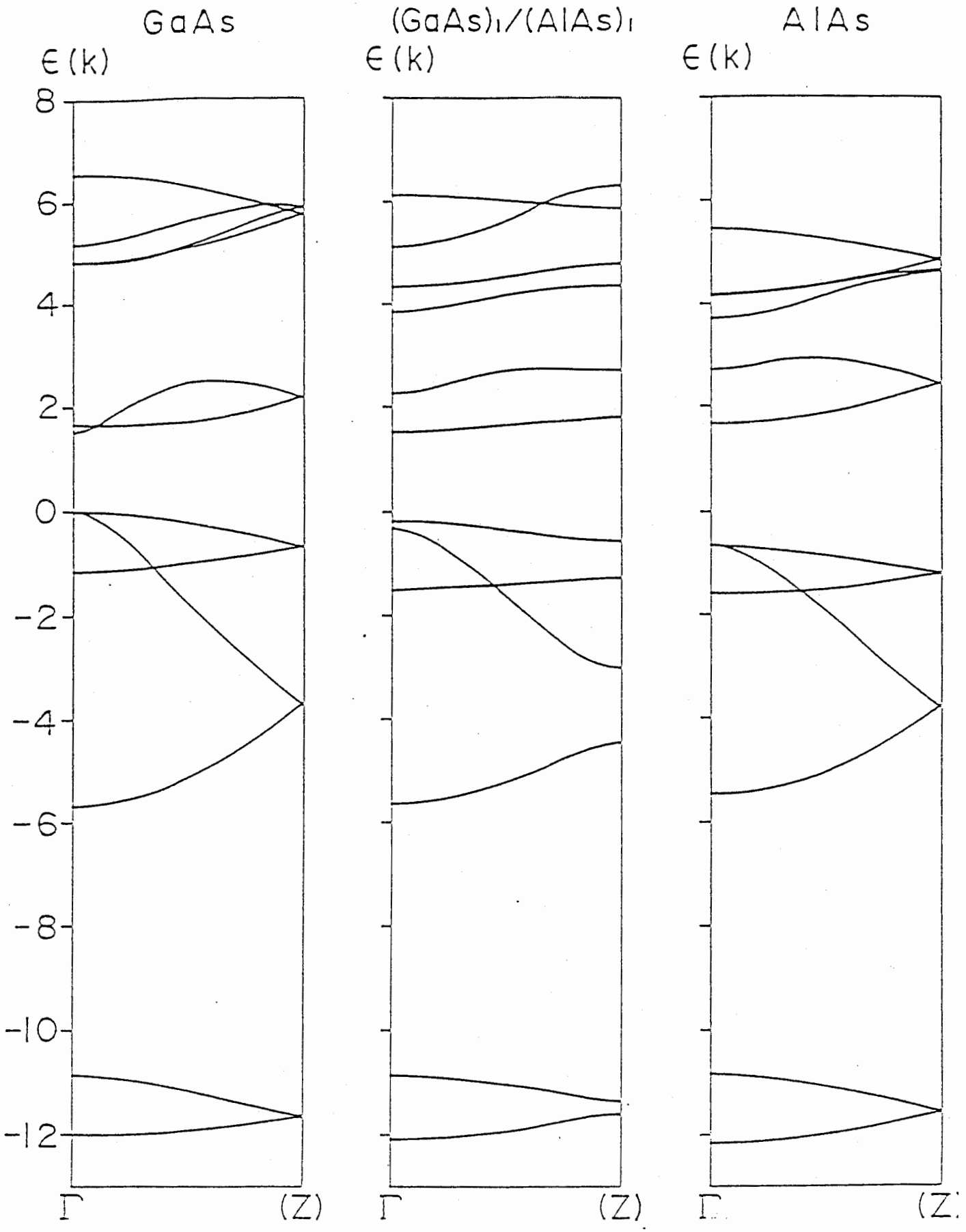

[111]
Supelattices

Fig 5.7

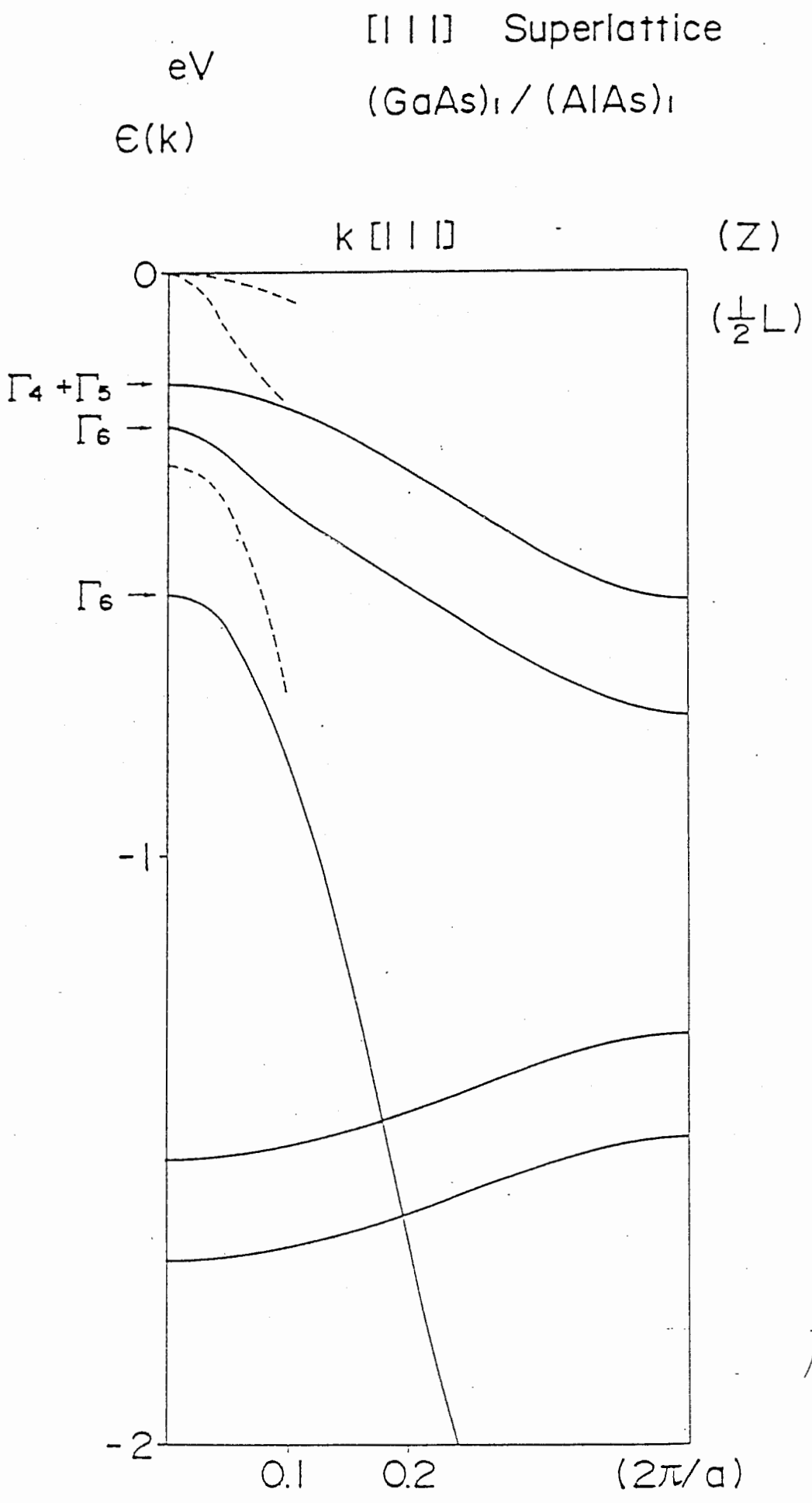
[1 1 1] Superlattice
(GaAs)1 / (AlAs)1
eV
ϵ(k)
k [1 1 1]
(Z)
(½L)
0
Γ4 +Γ5
Γ6
Γ6
-1
-2
0.1
0.2
(2π/a)

Fig. 5.8

Table Captions

Table 4.1 The irreducible representations of the double point group T_d and the character for the three bonding orbitals under the T_d symmetry with and without inclusion of the spin-orbit interaction.

Table 4.2 The irreducible representations of the double point group D_{2d} and the character for the three bonding orbitals under the D_{2d} symmetry with and without inclusion of the spin-orbit interation.

Table 5.1 The irreducible representations of the double point group C_{3v} and the reduction of representation consisting of the three bonding *p*-like orbitals under the C_{3v} symmetry with and without inclusion of spin-orbit interaction. Note that the basis functions of Γ_4, Γ_5 and Γ_6 are represented by making use of the eigenfunctions of the total angularmomentum, J and Jz, for instance, $|\ 1/2, 1/2\ \rangle$ is the eigenfunction of $J = 1/2$ and $Jz = 1/2$.

T_d	E	$6IC_4$	$3C_2$	$6\sigma_d$	$8C_3$
A_1 Γ_1	1	1	1	1	1
A_2 Γ_2	1	−1	1	−1	1
E Γ_3	2	0	2	0	−1
T_1 Γ_4	3	1	−1	−1	0
T_2 Γ_5	3	−1	−1	1	0
$E_{1/2}$ Γ_6	2 −2	$\sqrt{2}$ $-\sqrt{2}$	0	0	1 −1
$E_{5/2}$ Γ_7	2 −2	$-\sqrt{2}$ $\sqrt{2}$	0	0	1 −1
$G_{3/2}$ Γ_8	4 −4	0 0	0	0	−1 1
$\{P_i\}$	3	−1	−1	1	0
$\{P_i\}\times E_{1/2}$	6 −6	$-\sqrt{2}$ $\sqrt{2}$	0	0	0

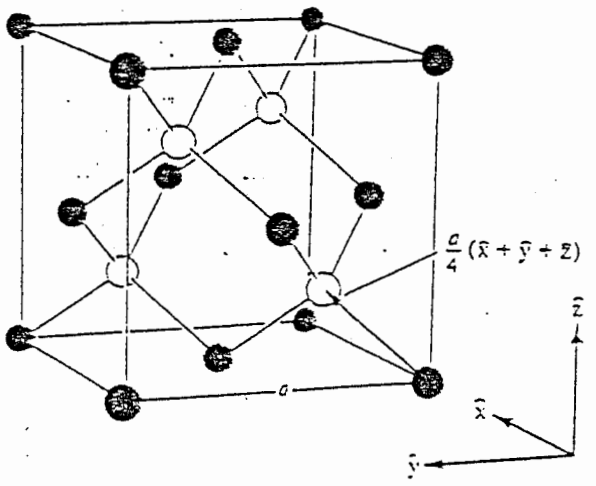

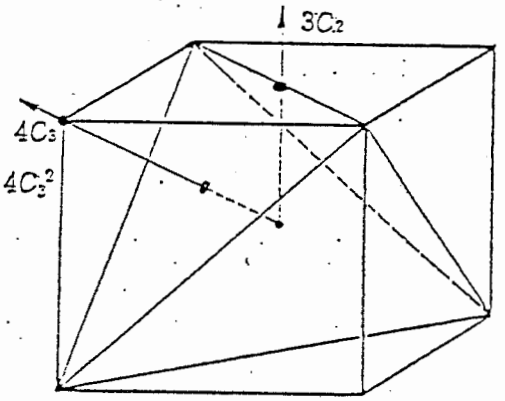

点群 T に属する回転対称操作

Table 4.1

D_{2d}		E	$2IC_4$	C_2	$2C_2'$	$2\sigma_d$
A_1 Γ_1	z^2, xyz	1	1	1	1	1
A_2 Γ_2	$z(x^2-y^2)$	1	1	1	−1	−1
B_1 Γ_3	x^2-y^2	1	−1	1	1	−1
B_2 Γ_4	z, xy	1	−1	1	−1	1
E Γ_5	$\{x, y\}$	2	0	−2	0	0
$E_{1/2}$ Γ_6	$\{\alpha, \beta\}$	2 −2	$\sqrt{2}$ $-\sqrt{2}$	0	0	0
$E_{3/2}$ Γ_7	$\{z\alpha, z\beta\}$	2 −2	$-\sqrt{2}$ $\sqrt{2}$	0	0	0
$\{P_i\}$		3	−1	−1	−1	1
$\{P_i\}\times E_{1/2}$		6 −6	$-\sqrt{2}$ $\sqrt{2}$	0	0	0

Tafle 4.2

Table 5.1

C_{3v}	E	$2C_3$	$3\sigma_v$	
A_1 Γ_1	1	1	1	z
A_2 Γ_2	1	1	−1	J_z
E Γ_3	2	−1	0	(x, y)
$E_{1/2}$ Γ_6	2 −2	1 −1	0	$\begin{cases} \lvert 1/2, 1/2 \rangle \\ -\lvert 1/2, -1/2 \rangle \end{cases}$ $\begin{cases} \lvert 3/2, 1/2 \rangle \\ \lvert 3/2, -1/2 \rangle \end{cases}$
$E_{3/2}$ Γ_4	1 −1	−1 1	i $-i$	$-\lvert 3/2, 3/2 \rangle - i \lvert 3/2, -3/2 \rangle$
$E_{3/2}$ Γ_5	1 −1	−1 1	$-i$ i	$-\lvert 3/2, 3/2 \rangle + i \lvert 3/2, -3/2 \rangle$
$\chi(\{P_i\})$	3	0	1	$\Gamma_1 + \Gamma_3$
$\chi(\{P_i\}) \times E_{1/2}$	6 −6	0 0	0 0	$2\Gamma_6 + \Gamma_4 + \Gamma_5$